https://doi.org/10.5194/egusphere-2025-5721
Preprint. Discussion started: 23 January 2026

A Preliminary Study on a Synergistic Assimilation Scheme for Multi-band Satellite Soil Moisture Data

Xuesong Bai[1], Zhaohui Lin[2], Zhengkun Qin[1], Juan Li[3,4]

[1]State Key Laboratory of Climate System Prediction and Risk Management, Nanjing University of Information Science and Technology, Nanjing, 210044, China; 202311010004@nuist.edu.cn (X.B.); qzk_0@nuist.edu.cn (Z.Q.)
[2]International Center for Climate and Environment Sciences, Institute of Atmospheric Physics, Chinese Academy of Sciences, Beijing, 100029, China
[3]CMA Earth System Modeling and Prediction Centre, Beijing, 100081, China; lj@cma.gov.cn
[4]State Key Laboratory of Severe Weather, Chinese Academy of Meteorological Sciences, Beijing, 100081, China

Correspondence to: Zhaohui Lin (lzh@mail.iap.ac.cn)

Abstract. Soil moisture retrievals from satellite sensors operating at different microwave frequencies provide diverse and complementary data sources for assimilation. However, fully exploiting the advantages of each frequency band while increasing the volume of assimilated observations remains a challenge. This study assimilates soil-moisture retrievals from three dominant-frequency instruments—SMAP (Soil Moisture Active–Passive), ASCAT (Advanced Scatterometer), and MWRI (Microwave Radiation Imager)—into the Common Land Model (CoLM) via the Simplified Extended Kalman Filter (SEKF). On the basis of a systematic assessment of the disparate impacts of each single-band product, we propose and test a synergistic multi-satellite assimilation framework that optimally combines the complementary information inherent in the multi-frequency observations. Results show that assimilating soil-moisture retrievals significantly improves the accuracy of the CoLM land-surface model; nevertheless, the effectiveness of each product exhibits a pronounced dependency on vegetation type. Analyses of simultaneous multi-source assimilation indicate that, when SMAP and ASCAT products are already ingested, the additional introduction of MWRI data over low-stature vegetation further enhances the joint assimilation performance. Validation against in-situ observations across China demonstrates that the largest improvements occur in the central and western parts of the country: the domain-mean correlation coefficient rises by about 0.25, while the error declines from 0.068 to 0.058 m^3m^{-3}. This indicates that improvements from multi-sensor assimilation stem not only from increased data volume but also from the complementary characteristics of the assimilated products. These findings provide valuable insights into the design of synergistic multi-sensor land data assimilation systems and contribute to improving land surface modeling, as well as weather and climate prediction accuracy.

1 Introduction

Soil moisture is a critical component of the terrestrial water and energy cycles, exerting strong influences on agricultural productivity, weather and climate prediction, water resources management, and climate change (Seneviratne et al., 2010; Taylor, 2015; Wanders et al., 2019b; Zhang et al., 2002). In the climate system, soil moisture primarily modulates the

https://doi.org/10.5194/egusphere-2025-5721
Preprint. Discussion started: 23 January 2026

partitioning of surface sensible and latent heat fluxes, thereby directly influencing the energy exchange processes involved in land–atmosphere interactions (Lin et al., 2010; Zhan and Lin, 2011; Zhou et al., 2020). Because soil moisture has memory properties, soil moisture anomalies can persist from weeks to months (Koster et al., 2020; 詹艳玲 et al., 2020). This providing a crucial source of predictability for sub-seasonal to seasonal forecasts, particularly in the context of extreme events such as droughts and heatwaves (Zhou et al., 2019). In weather systems, soil moisture changes the thermodynamic structure of the near-surface atmospheric boundary layer, which influencing precipitation patterns. It also plays a critical role in triggering deep convection by modulating atmospheric stability (Taylor, 2015; Wanders et al., 2019a)

Land surface models (LSMs) provide one of the primary means for estimating soil moisture with high spatiotemporal continuity. Improving LSM accuracy is essential for producing reliable soil moisture estimates, advancing understanding of land–atmosphere interactions, and enhancing the skill of weather and climate forecasts in coupled land–atmosphere modeling systems (Dai et al., 2003; Lawrence et al., 2019).

Optimizing initial conditions is a crucial method to improving model performance. Through data assimilation combined with soil moisture observations, one can obtain initial conditions that are closest to the truth and suitable for the model. The effectiveness of data assimilation improvements primarily depends on accurate observational data. Although the International Soil Moisture Network (ISMN) integrates in situ measurements from multiple countries to provide long-term time series of multi-layer soil moisture (Dorigo et al., 2021), the high spatial heterogeneity of soil moisture makes it difficult to comprehensively represent regional or global conditions based solely on limited in-situ data.

Over the past few decades, satellite-based microwave remote sensing of soil moisture has made significant progress, becoming the primary source for continuous, large-scale soil moisture data. Microwave sensors can penetrate clouds and atmospheric aerosols, enabling the acquisition of surface information under most weather conditions. Differences in the dielectric properties of wet and dry soils enable the retrieval of soil moisture. Using microwave observations across different frequency bands, various soil moisture products have been developed. Passive microwave instruments that can be used for soil moisture retrieval typically operate in the X-, C-, and L-band frequencies, such as the X-band MWRI (Kang et al., 2021; Zhu et al., 2019), C-band SMMR (Njoku et al., 1980), AMSR-E (Njoku et al., 2003), AMSR2 (Parinussa et al., 2015), and the L-band SMOS (Kerr et al., 2012). Active microwave sensors mainly include the C-band AMI Scatterometer (Zribi, 2003), ASCAT (Bartalis et al., 2007; Zhao et al., 2021), and Sentinel-1 SAR (Paloscia et al., 2013). Furthermore, the SMAP satellite combines L-band active and passive microwave sensing to further enhance the accuracy of soil moisture retrieval (Entekhabi et al., 2010).

Considerable progress has been achieved in data assimilation studies using various satellite-retrieved datasets (Draper et al., 2009; Kumar et al., 2006, 2009, 2014; Lin et al., 2017; Liu et al., 2013; Santanello et al., 2016). AMSR retrieval data have been widely used in assimilation studies with LSM such as SiB2 and CLM4.5, significantly improving the simulation accuracy of variables like soil moisture, evapotranspiration, and surface runoff (Draper and Reichle, 2015; Liu and Mishra, 2017). Many studies based on the Ensemble Kalman Filter (EnKF) have demonstrated the positive impact of assimilating ASCAT-retrieved soil moisture on land surface and flood prediction models (Brocca et al., 2012; Shan et al., 2024; Wanders

https://doi.org/10.5194/egusphere-2025-5721
Preprint. Discussion started: 23 January 2026

et al., 2019b). Regarding SMAP data, Tian et al. (2023) demonstrated that assimilation of SMAP products not only enhanced land surface model forecasts but also improved parameter estimation. Shen et al. (2024) employed an image-based data assimilation approach to enhance the spatial distribution characteristics of soil moisture over inland East Asia.

However, owing to limitations in sensor capabilities and insufficient satellite orbital coverage, remote-sensing data provided by any single instrument inevitably exhibit certain deficiencies. Passive microwave sensors provide broad coverage but coarse resolution (tens of kilometers), making it difficult to resolve local-scale variability (Das et al., 2023; Njoku and Entekhabi, 1996). Active microwave sensors offer finer resolution but lower temporal sampling due to long revisit periods. Moreover, the sensitivity of different microwave frequencies (L-, C-, and X-bands) to soil moisture varies with vegetation, surface roughness, and soil properties, leading to differences in retrieval accuracy and assimilation performance. For example, L-band missions (SMOS, SMAP) penetrate vegetation well but exhibit larger errors over complex terrain (Wigneron et al., 2017). C-band sensors (ASCAT, Sentinel-1) have high temporal resolution but variable accuracy across vegetation types and seasons (Chen et al., 2018; El Hajj et al., 2017). X-band sensors perform well over bare soil but suffer increased errors in vegetated areas due to strong scattering (Kang et al., 2021).

With growing interest in satellite remote sensing, many countries have launched polar-orbiting meteorological satellites carrying microwave imagers, forming a global collaborative observation network (Peng et al., 2021; Piepmeier et al., 2017). Atmospheric data assimilation studies have shown that combining observations from multiple satellites with complementary orbits and sensing characteristics can increase coverage by more than 20%, enhancing assimilation performance and improving numerical weather prediction (Chambon et al., 2023; Li et al., 2024; Zapotocny et al., 2007). In contrast, multi-satellite synergistic assimilation in the land domain, particularly for soil moisture, remains limited. Existing studies have largely emphasized the benefit of increased data volume (Khaki et al., 2019; Kolassa et al., 2017; Seo et al., 2021), while paying less attention to exploiting the unique strengths of products from different frequency bands. Current schemes often adopt a unified error, ignoring differences in vegetation penetration and surface sensitivity among microwave sensors (Dash and Sinha, 2019), which may introduce errors from mismatched observation characteristics. Although, algorithm advances have narrowed the technical accuracy gap among soil moisture retrievals from different frequencies, the intrinsic physical properties of the instruments remain (Dorigo et al., 2010). The key distinction lies in vegetation penetration, L-band sensors penetrate vegetation well and perform best in moderately vegetated areas; C-band sensors have moderate penetration and are sensitive to vegetation changes; X-band sensors have weak penetration and mainly capture near-surface signals (Jackson and Schmugge, 1991; Kerr et al., 2010; Owe et al., 2001). Therefore, this study first quantifies the vegetation-type-dependent heterogeneity in the assimilation efficacy of diverse satellite retrievals, thereby delineating the relative advantages associated with each spectral band. Building on this insight, a vegetation-aware multi-satellite data-assimilation framework will be formulated to harness complementary observational information and engender synergistic improvements, ultimately advancing the accuracy of numerical prediction.

https://doi.org/10.5194/egusphere-2025-5721
Preprint. Discussion started: 23 January 2026

The remainder of this paper is organized as follows. Section 2 details the data used in this study. Section 3 describes the CoLM, the SEKF method, and the corresponding experimental design. Section 4 presents and discusses the numerical results in detail. Finally, Section 5 summarizes the main conclusions of the study.

2 Datasets

2.1 Satellite datasets

Informed by the complementary strengths of active and passive microwave sensing at divergent frequencies, this study assimilates soil-moisture retrievals from three mainstream sensors: the U.S. Soil Moisture Active Passive (SMAP), the European Advanced Scatterometer (ASCAT), and China's Microwave Radiation Imager (MWRI). The data period covers June to August 2022.

The SMAP soil moisture retrievals were obtained from the Level-2 L2_SM_P_E product provided by the National Snow and Ice Data Center (NSIDC), USA (ONeill et al., 2023). The product is available at multiple horizontal resolutions; the 36-km dataset is adopted here.

ASCAT retrievals are obtained from the Advanced Scatterometer carried on the Metop satellite series launched by the European Organisation for the Exploitation of Meteorological Satellites (EUMETSAT), which provides global soil moisture estimates via C-band radar backscatter (Bartalis et al., 2007). This study uses the ASCAT H SAF H113 product with a spatial resolution of 12.5 km. Soil moisture is retrieved using a change detection algorithm that links radar backscatter variations to soil moisture changes. Volumetric water content is then obtained by converting soil water saturation using porosity data from the ESA-CCI (European Space Agency Climate Change Initiative).

The MWRI soil moisture data are from a dataset developed by the National Satellite Meteorological Center of China Meteorological Administration (CMA) (Kang et al., 2021). The MWRI instrument aboard the FY-3D satellite provides global microwave radiation measurements twice daily. The daily soil moisture product, with a horizontal resolution of 25 km on an EASE-Grid projection, integrates data from ascending and descending orbits. Surface soil moisture is retrieved from MWRI channel brightness temperature using a retrieval model.

Given that the spatial resolution of satellite products exceeds that of the LSM (about 1.4°×1.4°), all satellite soil moisture retrievals within each model grid cell were spatially averaged to prevent introducing excessive small-scale variability. The resulting spatially averaged soil moisture distribution is shown in Figure 1.

https://doi.org/10.5194/egusphere-2025-5721
Preprint. Discussion started: 23 January 2026

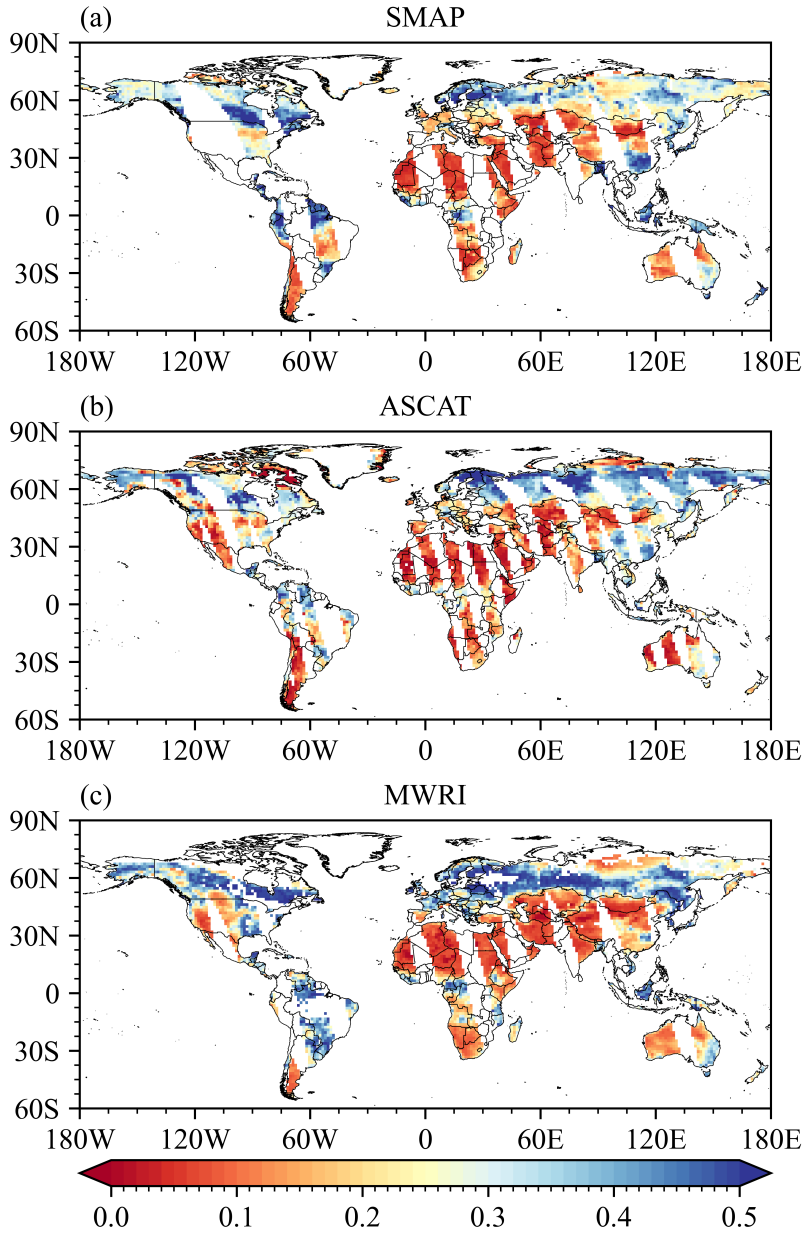

125 **Figure 1: Spatial distribution of grid-averaged soil moisture on June 2, 2022, from (a) SMAP, (b) ASCAT, and (c) MWRI.**

2.2 In-Situ Data

In-situ data were selected to validate the assimilation results. Soil moisture and precipitation observations were obtained from the ISMN and the CMA station network. The ISMN comprises over 1,400 stations across 35 international networks (Dorigo et al., 2021). The CMA network includes more than 2,400 surface meteorological stations in China, with

https://doi.org/10.5194/egusphere-2025-5721
Preprint. Discussion started: 23 January 2026

approximately 600 equipped with soil moisture and soil temperature sensors. For this study, soil moisture observations at 10 cm depth were used.

2.3 ERA5-Land Reanalysis Data

To improve the global applicability of validation, this study incorporates the ERA5-Land dataset developed by the European Centre for Medium-Range Weather Forecasts (ECMWF) under the Copernicus Climate Change Service (C3S) (Muñoz-Sabater, 2019). ERA5-Land is a high-resolution enhancement of the ERA5 reanalysis, focusing on land surface variables. Its soil moisture product includes four layers (0–7 cm, 7–28 cm, 28–100 cm, and 100–289 cm) providing volumetric water content.

3 Model and Experimental Design

3.1 CoLM model

This study uses the CoLM to simulate land surface processes. Developed primarily by Chinese research institutions, CoLM originated from integrating the IAP94 and CLM frameworks through collaboration between the Institute of Atmospheric Physics, Chinese Academy of Sciences, and NCAR. The model represents coupled soil hydrothermal and vegetation ecophysiological processes, and is widely applied in Earth system studies. We use the 2014 version, which incorporates major advances in soil physics and vegetation parameterizations, including an updated soil hydraulic scheme and a two-big-leaf canopy model. The model consists of 10 vertically stratified soil layers from the surface to bedrock. Soil moisture is simulated by numerically solving the Richards equation, accounting for root uptake, infiltration, and surface and subsurface runoff. Vegetation processes follow a plant functional type (PFT) approach, with a two-big-leaf scheme separating sunlit and shaded leaves to better represent canopy radiative and energy transfer (Dai et al., 2003; Li et al., 2017). Hydrological processes include precipitation interception, infiltration, evapotranspiration, and runoff generation, with subgrid-scale heterogeneity in topography, soil, and vegetation types explicitly considered.

3.2. CoLM Atmospheric Forcing

The atmospheric forcing data are derived from the ERA5 near-surface atmospheric variables, including downward shortwave and longwave radiation, precipitation, air pressure, specific humidity, air temperature, and wind speed. A bilinear interpolation method was used to interpolate the ERA5 data from its original 0.25° horizontal resolution to a 1.4°. The data have a temporal resolution of 3 hours and cover the period from January 1, 1979, to December 31, 2022. The numerical solution employs an explicit finite-difference method with a time step of 30 minutes to ensure simulation stability and accuracy. Model outputs, which include soil temperature, moisture, surface fluxes, evapotranspiration, and runoff, provide the basis for subsequent data assimilation and evaluation.

https://doi.org/10.5194/egusphere-2025-5721
Preprint. Discussion started: 23 January 2026

3.3. SEKF assimilation system

To accommodate the strong nonlinearities characteristic of land-surface processes, the Simplified Extended Kalman Filter (SEKF)—an assimilation scheme that dispenses with the adjoint model—is employed herein for soil-moisture data assimilation. SEKF was proposed by Hess (2001) and Balsamo et al. (2004) based on the Extended Kalman Filter (EKF). It approximates the derivative of the nonlinear observation operator by adding appropriate perturbations, thereby avoiding the development of a cumbersome adjoint model. Compared to the EKF, SEKF does not require local linearization of model equations and updates the observation operator gradient in real time, thereby retaining some flow-dependent error characteristics. The method is computationally efficient and has been implemented in land data assimilation systems such as that of ECMWF (Drusch et al., 2009; Herbert et al., 2024).

The analysis update step of the SEKF is consistent with the Kalman filter. First, the state is updated by weighting the difference between the observation and the simulated observation (i.e., Observation-Minus-Background, OMB) with the Kalman gain matrix **K**:

$$\boldsymbol{x}^{\mathrm{a}} = \boldsymbol{x}^{\mathrm{b}} + \mathbf{K}\left[\boldsymbol{y} - \boldsymbol{\mathcal{H}}\left(\boldsymbol{x}^{\mathrm{b}}\right)\right] \quad (1)$$

Here, $\boldsymbol{x}^{\mathrm{a}}$is the analysis state, $\boldsymbol{x}^{\mathrm{b}}$ is the background state, $\boldsymbol{y}$ is the observation, $\boldsymbol{\mathcal{H}}$ is the nonlinear observation operator. The Kalman gain matrix **K** is computed as follows:

$$\mathbf{K} = \mathbf{B}\mathbf{H}^{\mathrm{T}}(\mathbf{H}\mathbf{B}\mathbf{H}^{\mathrm{T}} + \mathbf{R})^{-1} \quad (2)$$

B is the background error covariance, **R** is the observation error covariance, and **H** is the linearized observation operator. To account for the nonlinear nature of the observation operator in LSM, the SEKF computes **H** using a finite-difference perturbation approach. Specifically, a small perturbation $\delta\mathbf{x}_{\mathrm{j}}$ is applied to each component $\mathbf{x}_{\mathrm{i}}$ of the state vector, and the resulting change in the simulated observation is used to approximate the first-order derivative of the observation operator with respect to that state component:

$$\mathbf{H}_{\mathrm{ij}} = \frac{\boldsymbol{\mathcal{H}}(\mathbf{x}_{\mathrm{i}}+\delta\mathbf{x}_{\mathrm{i}}) - \boldsymbol{\mathcal{H}}(\mathbf{x}_{\mathrm{i}})}{\delta\mathbf{x}_{\mathrm{j}}} \quad (3)$$

The observation operator is estimated using the finite-difference approach described above. Each perturbation must be small enough to satisfy the linear approximation yet large enough to avoid numerical noise. Based on previous research (Bai et al., 2025), perturbations of 0.001, 0.0001, 0.0001, 0.0001, 0.0005, 0.001, and 0.0005 m^3m^{-3} are applied to the top seven soil layers, respectively. Consistent with Albergel et al. (2017), the retrieved soil moisture from satellite products is mapped to the model's second soil layer.

3.4. Experiment design

The primary objective of this study is to quantify the extent to which assimilating diverse soil-moisture retrievals can enhance the shill of the CoLM in simulating the land surface variables. To ensure the deep-layer soil variables reached a

https://doi.org/10.5194/egusphere-2025-5721
Preprint. Discussion started: 23 January 2026

statistical equilibrium, the model was first spun up for 342 years from a cold start. Subsequently, a series of sensitivity experiments were designed to quantify the assimilation efficacy of different soil moisture products.

Three groups of numerical experiments were conducted. The first is a control experiment (CTL), serving as a reference benchmark. In CTL, the CoLM was integrated from a hot start for two months (2 June–1 August 2022) without data assimilation. In the second experiment suite, the SEKF assimilation module is activated to sequentially ingest SMAP-, ASCAT-, and MWRI-derived soil-moisture products, designated as the L, C, and X experiments, respectively. Each experiment consists of one month of daily assimilation cycles, followed by a one-month free forecast. Observations were assimilated once daily at 0000 UTC. Following Bai et al. (2025), observation and background error statistics were derived from the RMSE between CTL and ERA5 reanalysis during June–August 2022. The third group of experiments was conducted to investigate the effects of continuous data assimilation on model performance in simulating the soil moisture. This set involved continuous assimilation over the entire two-month study period, encompassing the assimilation of single datasets (L, C, and X), their pairwise combinations (L+C, L+X, C+X), and all three datasets simultaneously (L+C+X). A summary of all experiment configurations is provided in Table 1.

Table 1. Experiment design.

Group	Experiment	Assimilated product(s)	Assimilation phase	Forecast phase
One	CTL			20220602-20220801
Two	L	SMAP	20220602-20220703	20220703-20220801
	C	ASCAT	As above	As above
	X	MWRI	As above	As above
Three	L	SMAP	20220602-20220801	
	C	ASCAT	As above	
	X	MWRI	As above	
	L+C	SMAP+ASCAT	As above	
	L+X	SMAP+MWRI	As above	
	C+X	ASCAT+MWRI	As above	
	L+C+X	SMAP+ASCAT+MWRI	As above	

4. Results

4.1. Comparison of Assimilation Performance for Different Frequency Bands

Comparing Group 1 (CTL) and Group 2 (assimilation experiments) clarifies the forecast improvements from land data assimilation. ERA5-Land soil moisture is used to quantify the effect of assimilating L-, C-, and X-band satellite retrievals on the simulations. Figure 2 shows spatial correlation coefficients (R) and root-mean-square error (RMSE) relative ERA5-Land.

https://doi.org/10.5194/egusphere-2025-5721
Preprint. Discussion started: 23 January 2026

Assimilation from all three bands improves soil moisture accuracy across 0–1 m, with band- and depth-dependent magnitudes. C-band yields the largest gains, R increases by 0.15, 0.12, and 0.09 and RMSE decreases by 0.020, 0.015, and 0.012 m^3m^{-3} for the 0–7 cm, 7–28 cm, and 30–100 cm layers, respectively. L-band ranks second in performance and exhibits clear depth-dependent variations. At the surface layer, its ΔR reaches 0.13, which exceeds that of X-band (0.11). In the second layer, the improvements are comparable between the two, while in the third layer, L-band performs slightly worse than X-band. In the forecast phase, the results differ from those in the assimilation phase. L-band shows the smallest improvement in both R and RMSE, suggesting a more rapid loss of its assimilation impact. In contrast, the effects of C- and X-band assimilation remain more persistent throughout the forecast period.

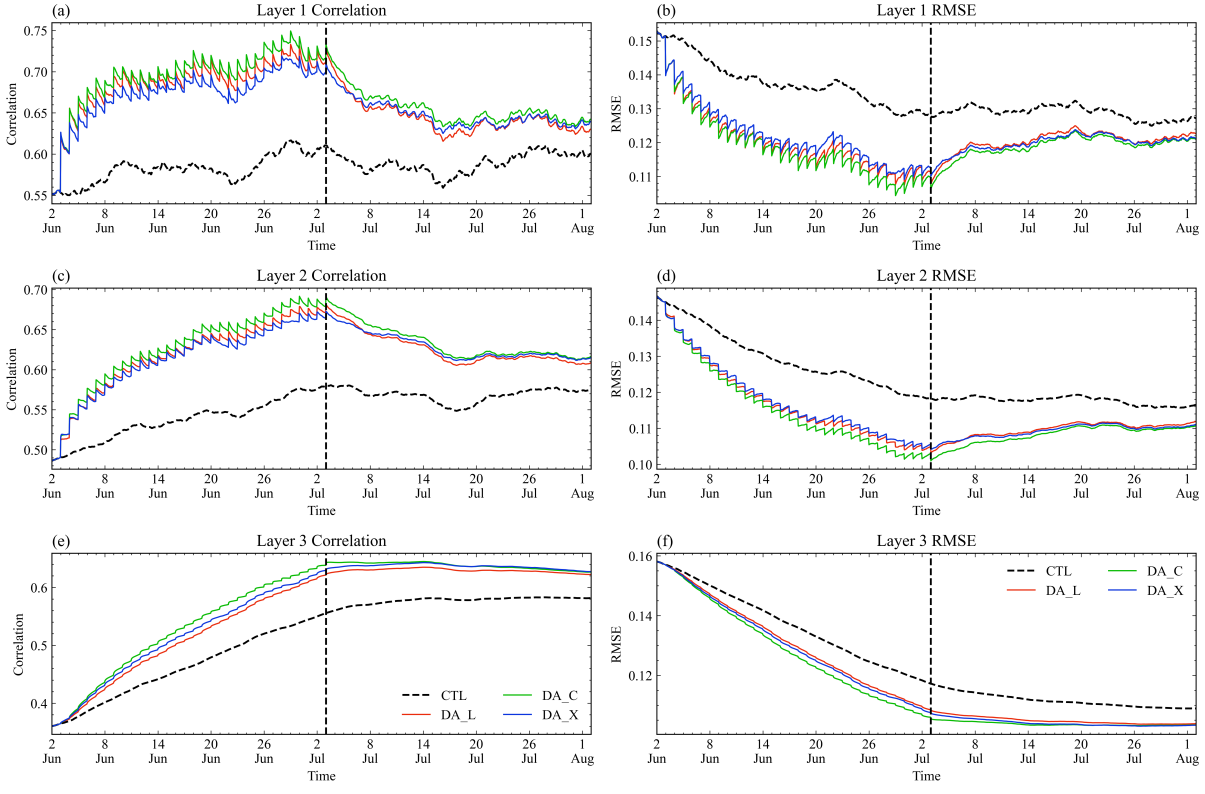

Figure 2: Spatial correlation coefficients (left panels) and RMSE (right panels) of soil moisture relative to ERA5-Land for different experiments. (a, c, e) is spatial correlation coefficients for layer 1, layer 2, and layer 3, respectively, and (b, d, f) is the corresponding RMSE for layer 1, layer 2, and layer 3, respectively. The region to the left of the vertical dashed line denotes the assimilation phase, and the region to the right denotes the forecast phase. The dashed line represents the CTL, while red, green, and purple lines represent the assimilation of L-, C-, and X-band soil moisture products, respectively.

To further explore the causes of performance differences among the frequency bands, the mean first-layer soil moisture is analyzed. As shown in Figure 3, the analysis fields exhibit notable spatial variations and a clear latitudinal dependence. Over southeastern China between 10°–30°N, all three experiments identify the region as having high soil moisture, yet the L experiment is comparatively wetter and in closer agreement with ERA5-Land. At higher latitudes, such as northern Canada

https://doi.org/10.5194/egusphere-2025-5721
Preprint. Discussion started: 23 January 2026

and Siberia, the dry–wet contrast is more pronounced in the X- and C-band experiments. However, the L-band experiment exhibits an overly dry bias that deviates from ERA5-Land. In the wetter regions of southeastern Australia, the X-band results most closely match ERA5-Land, while the C-band experiment displays a distinct dry bias. These results indicate that the assimilation performance of different frequency bands exhibits strong regional dependence.

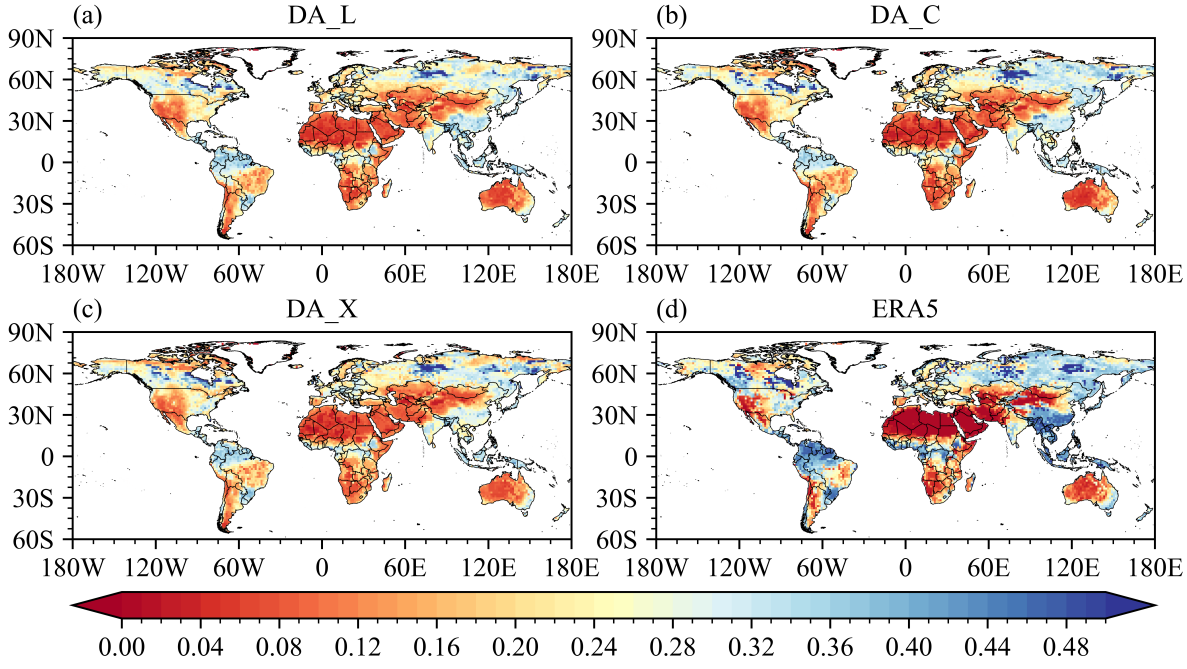

Figure 3: Spatial distribution of mean soil moisture in the top layer during 2 June to 3 July 2022. (a)–(c) show the analysis fields from the L-, C-, and X-band assimilation experiments, respectively, and (d) shows the corresponding ERA5-Land soil moisture.

To further clarify the regional dependence of assimilation performance, the global land surface was divided into three latitudinal bands: 90°S–30°S, 30°S–30°N, and 30°N–90°N. Spatial correlation coefficients and RMSE were computed for each zone, as shown in Figure 4. In the CTL, the best model performance can be found in the tropics (30°S–30°N), where spatial correlation reached 0.8 and RMSE was approximately 0.115 m^3m^{-3}. In contrast, performance was poorest in the Northern Hemisphere (30°N–90°N), with correlation around 0.4 and RMSE exceeding 0.15 m^3m^{-3}.

Assimilation experiments show that in the Southern Hemisphere and tropical regions, the L-band provides the most notable improvement during both the assimilation and forecast phases. For example, in the 90°S–30°S band, the second-layer soil moisture correlation increased by 0.10 and RMSE decreased by 0.015 m^3m^{-3}. However, in the Northern Hemisphere (30°N–90°N), the C- and X-band experiments outperformed L-band assimilation. In particular, C-band assimilation improved the second-layer correlation by 0.16 and reduced RMSE by 0.024 m^3m^{-3} relative to the CTL, indicating the best performance in this region.

https://doi.org/10.5194/egusphere-2025-5721
Preprint. Discussion started: 23 January 2026

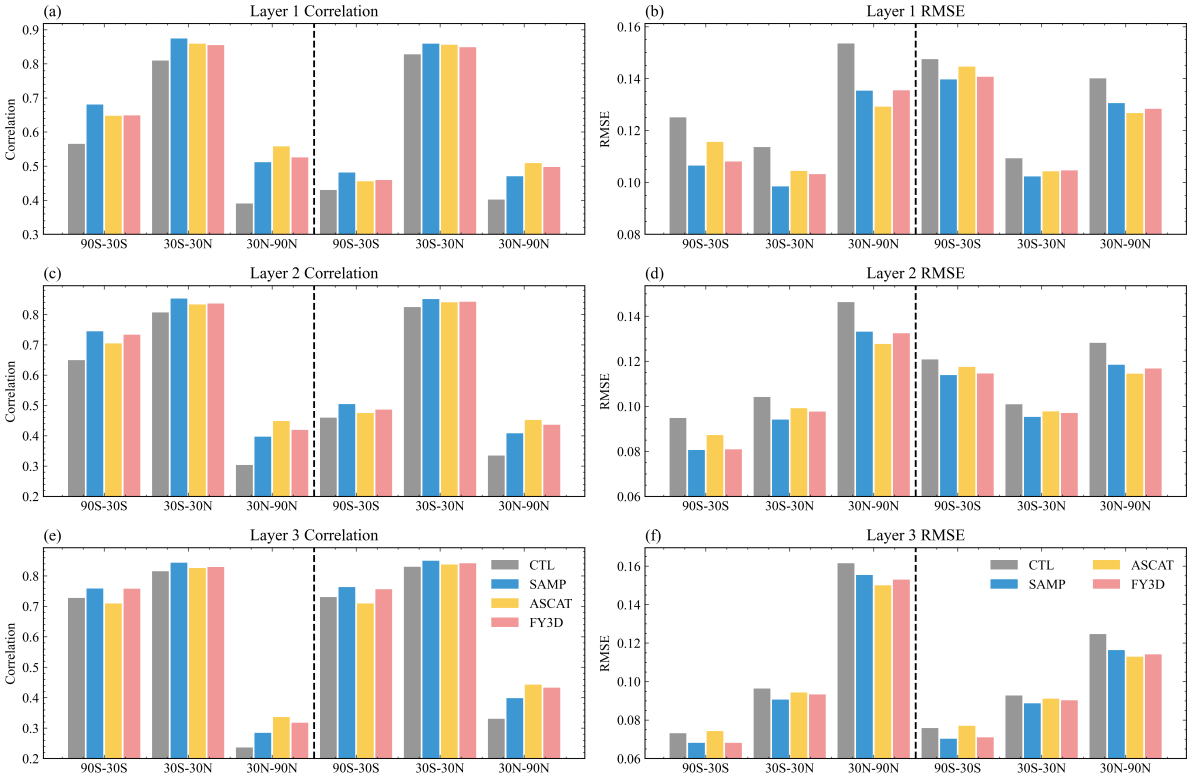

Figure 4: Spatial correlation coefficients (left panels) and RMSE (right panels) of soil moisture relative to ERA5-Land across different latitudinal zones for the four experiments. (a, c, e) is spatial correlation coefficients for layer 1, layer 2, and layer 3, respectively, and (b, d, f) is the corresponding RMSE for layer 1, layer 2, and layer 3, respectively. The left and right sides of the vertical dashed line correspond to the assimilation and forecast phases, respectively. Gray represents the control experiment, while blue, yellow, and pink represent assimilation of SMAP, ASCAT, and FY-3D soil moisture products, respectively.

Given the differing penetration capabilities of microwave frequencies and the strong correlation between vegetation density and latitude, variations in vegetation type likely contribute to the observed latitudinal differences in assimilation performance. Figure 5 shows the evaluation results of the assimilation experiments across different vegetation types, validated against ERA5-Land to ensure sufficient sample sizes. The vegetation types are arranged in order of increasing density. Assimilation of MWRI X-band data performs best in sparsely vegetated regions, with consistent improvements across all soil depths. In contrast, in densely vegetated areas, the deeper penetration of lower-frequency sensors becomes evident. SMAP (L-band) demonstrates the most stable performance, particularly in deeper soil layers. For example, in temperate broadleaf forests (BET Temperate), the improvement in correlation for deep-layer soil moisture exceeds that of the surface layer, while the X-band experiment exhibits a negative impact. These results align with findings from Mousa and Shu (2020), who used the Triple Collocation method and reported that SMAP significantly outperformed ASCAT in forested regions of Africa.

https://doi.org/10.5194/egusphere-2025-5721
Preprint. Discussion started: 23 January 2026

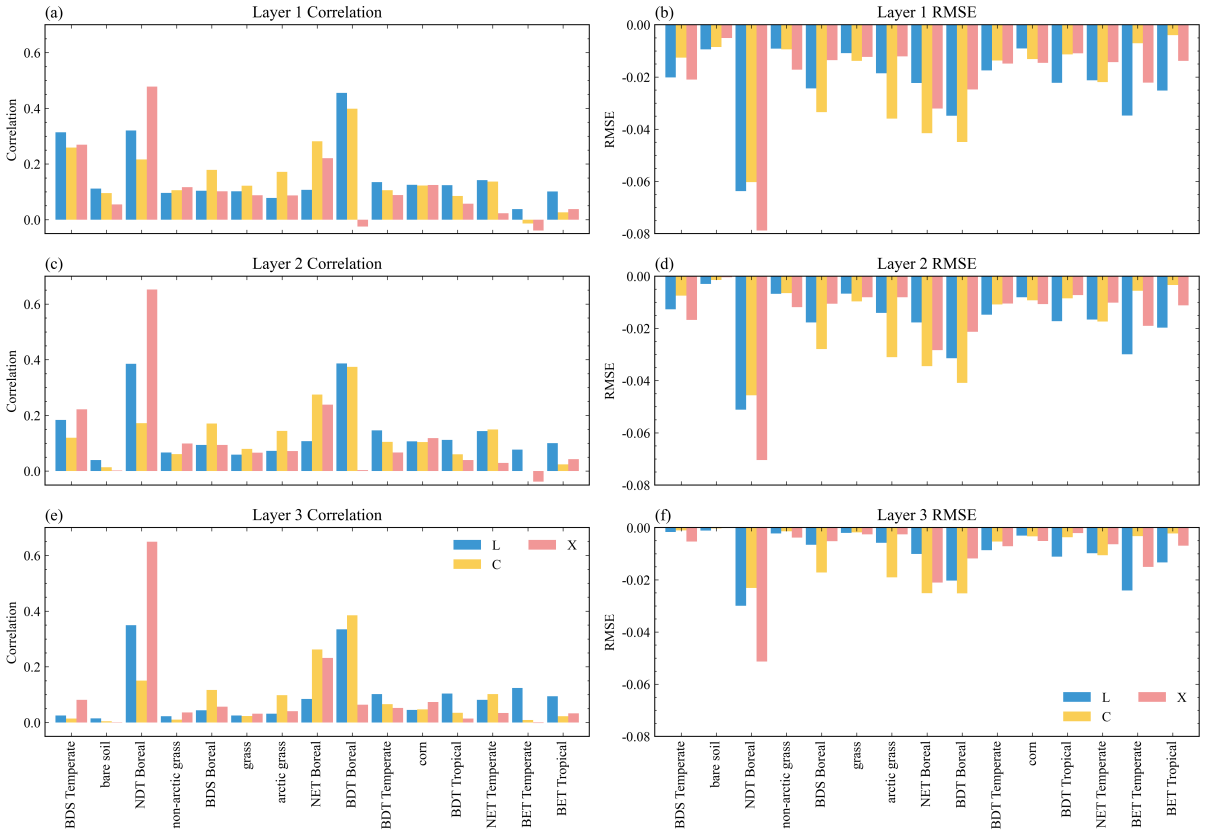

Figure 5: Changes in correlation coefficient (left panels; after-minus-before assimilation) and RMSE (right panels; after-minus-before assimilation) of soil moisture relative to ERA5-Land during 2 June to 3 July 2022, shown as a function of vegetation type. (a, c, e) is correlation coefficients for layer 1, layer 2, and layer 3, respectively, and (b, d, f) is the corresponding RMSE for layer 1, layer 2, and layer 3, respectively.

Recognizing that reanalysis data are not absolute truth, we further evaluated the assimilation performance using in situ observations from China. Figure 6 presents correlation and RMSE statistics for each experiment, ordered by increasing vegetation cover. Some vegetation types are omitted due to a lack of corresponding station data. The correlation results show that both L-band and C-band assimilation consistently improve model performance across all available vegetation types, except in the Arctic Grass region where RMSE increases slightly. Notably, in densely vegetated areas, assimilation of the MWRI product leads to a decline in correlation, highlighting its limited effectiveness under dense canopy conditions. These findings are consistent with the reanalysis-based evaluation and reinforce the robustness of the earlier conclusions.

https://doi.org/10.5194/egusphere-2025-5721
Preprint. Discussion started: 23 January 2026

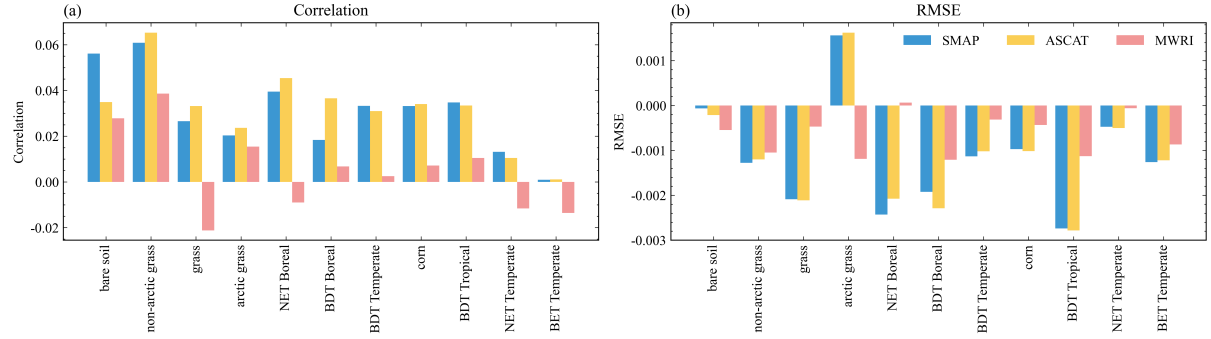

Figure 6: Same as Figure 5, but for comparison between model soil moisture and in situ observations at 0–10 cm depth. (a) is correlation coefficients for 0-l0 cm, and (b) is the corresponding RMSE for 0-10 cm.

As defined in the experimental design, the primary difference among the experiments lies in the observation data used. Given that all satellite products achieve near-global coverage during the one-month continuous assimilation period, differences in assimilation performance are largely attributed to observation errors. To explore the relationship between assimilation performance and vegetation type, we evaluated the retrieval accuracy of each satellite product using in situ soil moisture observations under different vegetation types. Figure 7 presents the correlation and RMSE of SMAP, ASCAT, and MWRI retrievals against in situ measurements, with vegetation types ordered as in Figure 5.

The retrieval accuracy of all three products exhibits a clear dependence on vegetation density. SMAP shows increasing correlation and decreasing RMSE with higher vegetation cover, reflecting the stronger canopy penetration capability of L-band radiometry. In contrast, ASCAT and MWRI retrievals degrade as vegetation density increases, performing best in sparsely vegetated and bare soil regions. These results suggest that spatial variations in assimilation performance are primarily driven by the intrinsic differences in retrieval accuracy among the products. The longer wavelength of the L-band enables SMAP to maintain high accuracy in densely vegetated areas, while C-band (ASCAT) and X-band (MWRI) retrievals are more strongly affected by vegetation-induced scattering and attenuation.

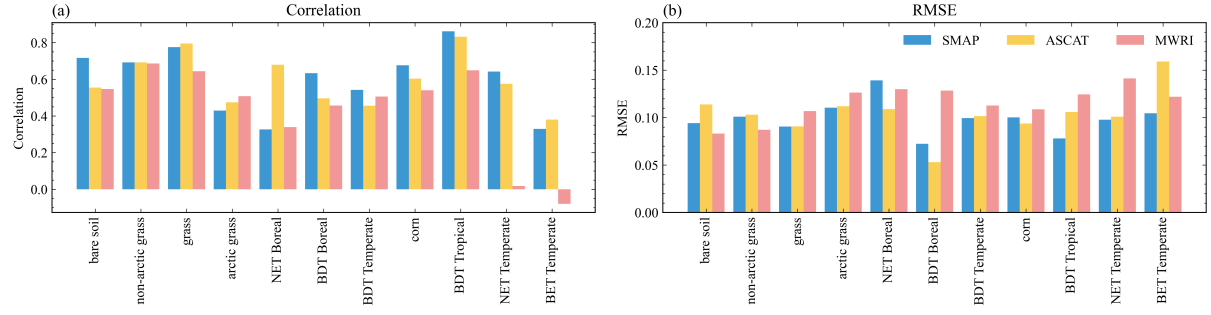

Figure 7: Correlation coefficients (a) and RMSE (b) between satellite-retrieved soil moisture and in situ observations. Light blue, orange, and red bars represent SMAP, ASCAT, and FY-3D products, respectively.

https://doi.org/10.5194/egusphere-2025-5721
Preprint. Discussion started: 23 January 2026

The vegetation-dependent differences in assimilation performance may help explain the pattern observed in Figure 2, where the impact of L-band assimilation decays more rapidly during the forecast phase. While L-band performs best in regions with dense vegetation and high precipitation (Mousa and Shu, 2020), soil moisture in these areas is frequently influenced by strong meteorological forcings such as rainfall. As a result, the assimilated information is more likely to be masked by subsequent hydrometeorological variability, leading to faster loss of forecast skill. In contrast, C- and X-band retrievals perform better in regions with low-to-moderate vegetation cover and more arid conditions (Sun et al., 2017). In these areas, less frequent precipitation and slower soil moisture dynamics allow the assimilated signal to persist longer, resulting in better forecast retention.

4.2. Synergistic Assimilation Performance Analysis

The preceding analyses demonstrate marked disparities in the assimilation efficacy of individual satellite products, underscoring the imperative of simultaneous multi-satellite data assimilation. To quantify the incremental benefit of assimilating various satellite-data combinations, Figure 8 displays the probability density functions (PDFs) of the differences between the spatial correlation coefficients of soil-moisture analyses from each assimilation experiment and those from the control experiment, with correlations calculated against in-situ observations. All PDFs exhibit a pronounced positive skew, indicating that every assimilation experiment outperforms the control. Moreover, dual-satellite assimilation systematically surpasses single-satellite assimilation, corroborating the added value of synergistic multi-source data integration for enhanced assimilation efficacy. Among the combinations, the L+C experiment (SMAP + ASCAT) shows the best performance. This improvement is likely due to the complementary characteristics of L- and C-band sensors under varying vegetation conditions: L-band performs well in densely vegetated areas, while C-band is more effective in low-to-moderate vegetation environments. Together, they provide more balanced and robust performance across diverse land surface conditions. This is consistent with the findings of Kim et al. (2018), who employed a method based on maximizing the correlation coefficient to merge different soil moisture products. Their results indicated that SMAP exhibited broader compatibility with products from other frequency bands. Notably, in densely vegetated regions, the combination of SMAP and ASCAT outperformed other fusion schemes. However, assimilating all three satellite products (L+C+X) does not further improve performance over the L+C combination and, in some cases, leads to degradation. For example, the probability density function of performance metrics shows more frequent negative values in the L+C+X case compared to L+C. This suggests that the inclusion of lower-quality data can reduce overall assimilation effectiveness in multi-source systems.

https://doi.org/10.5194/egusphere-2025-5721
Preprint. Discussion started: 23 January 2026

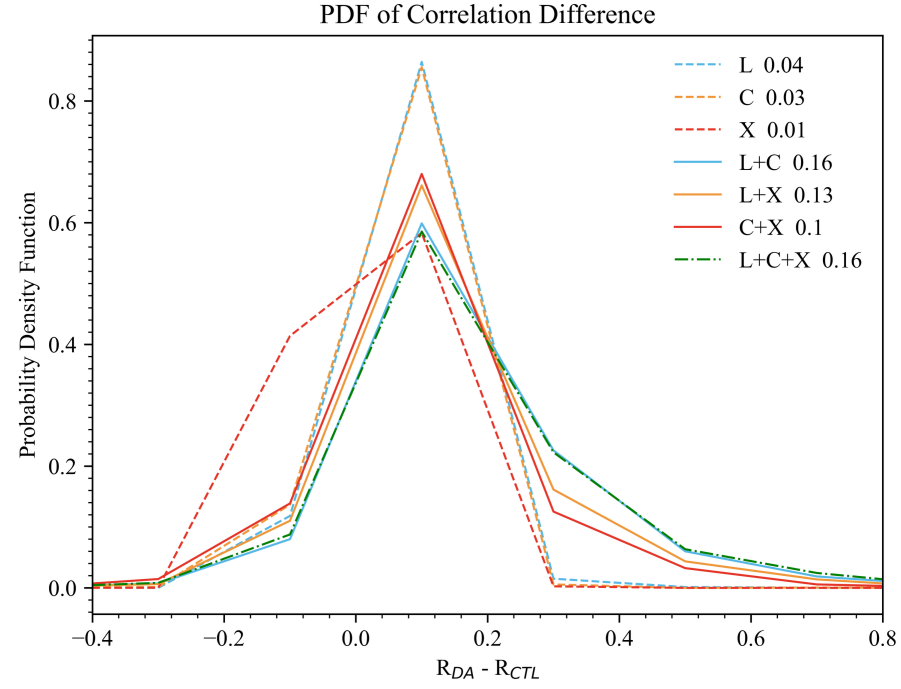

Figure 8: Probability density distributions of the correlation coefficient differences between assimilation experiments and the CTL, based on in situ observations. Legend values indicate the mean correlation improvement for each experiment.

To explain the negative impact observed when adding X-band data to the L+C combination, we analyzed a subset of representative vegetation types, Temperate Needleleaf Forest (NET Temperate), non-Arctic grassland, and corn. Figure 9 shows the changes in correlation and RMSE when a third satellite product is added to a two-source combination for each vegetation type. Adding SMAP (L-band) to the C+X combination led to consistent improvements across all three vegetation types, with increases in correlation and reductions in RMSE. This effect was most pronounced in non-Arctic grasslands, where correlation improved by 0.09 and RMSE decreased by 0.0015 m^3m^{-3}. Adding ASCAT (C-band) to the L+X combination also improved performance, though to a lesser extent. In contrast, incorporating MWRI (X-band) into the L+C combination produced minimal benefit and even reduced the correlation in the densely vegetated NET Temperate region.

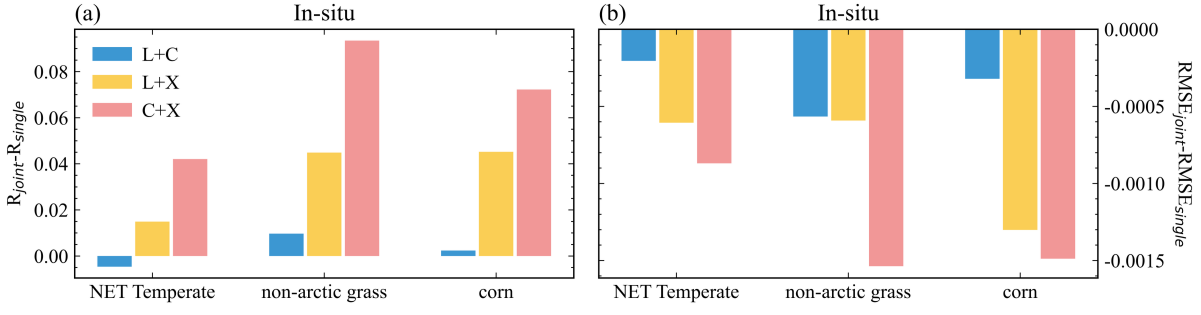

https://doi.org/10.5194/egusphere-2025-5721
Preprint. Discussion started: 23 January 2026

Figure 9: Changes in correlation coefficient (a) and RMSE (b) between model output and in situ observations after adding a third satellite product to each two-product assimilation combination, shown for selected vegetation types.

To better understand how vegetation influences the assimilation performance of different satellite products, a time-series validation was conducted using in situ observations. Figure 10 presents daily mean soil moisture from model simulations across different assimilation experiments, along with satellite retrievals and station observations. For the Corn vegetation type (Fig. 10c), the L+C+X experiment (DA_ALL) showed the highest accuracy, achieving a correlation of 0.83 with station data, compared to 0.56 for the control and 0.79 for the L+C experiment. The inclusion of X (FY-3D) data improved the model's ability to capture soil moisture responses to rainfall events, especially when L- and C-band data were unavailable on certain days (e.g., July 12). During the mid-July precipitation event, all experiments captured the sharp increase in soil moisture, but DA_ALL reproduced both the peak (July 11) and the subsequent dry-down (July 12–13) with greater fidelity. At the non-Arctic grassland site (Fig. 10b), FY-3D assimilation also contributed positively. The correlation in DA_ALL reached 0.43, compared to 0.23 for L+C. During the rainfall event on July 29, FY-3D provided supplementary data that compensated for missing L- and C-band inputs, enabling better simulation of daily moisture dynamics.

In contrast, a different pattern emerged in NET Temperature area (Fig. 10a). The time-series correlation for DA_ALL (0.53) was notably lower than that of L+C (0.63), consistent with the spatially averaged results. Between June 2 and June 20, FY-3D soil moisture exhibited a distinct pattern—first decreasing, then increasing, then decreasing again—while other products and in situ observations remained low and stable. The increase in soil moisture was only observed after continuous rainfall during July 5–10. The early divergence of FY-3D from both satellite and station observations led to erroneous updates during assimilation, degrading overall accuracy. This highlights the instability of the FY-3D product in densely vegetated environments, where signal scattering and attenuation significantly reduce retrieval reliability.

https://doi.org/10.5194/egusphere-2025-5721
Preprint. Discussion started: 23 January 2026

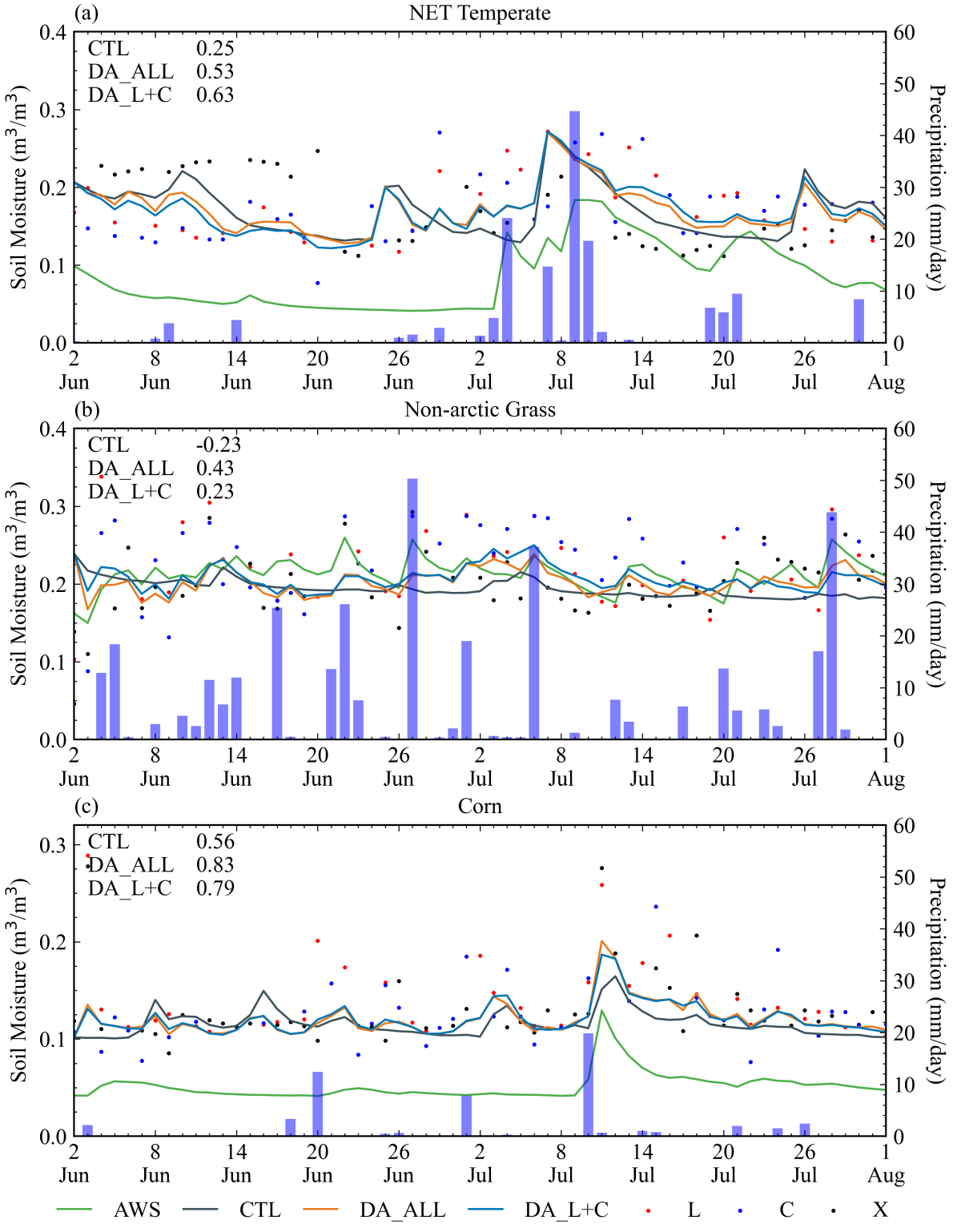

https://doi.org/10.5194/egusphere-2025-5721
Preprint. Discussion started: 23 January 2026

Figure 10: Time series of daily mean soil moisture from model simulations, satellite retrievals, and in situ observations for different assimilation experiments. The green solid line represents in situ observations. Black, orange, and blue solid lines indicate soil moisture simulations from the control experiment, the L+C+X assimilation experiment, and the L+C assimilation experiment, respectively. Red, blue, and black dots represent L-, C-, and X-band satellite soil moisture products, respectively. Blue bars denote daily precipitation.

The preceding analysis demonstrates that adding more satellite products does not necessarily lead to improved assimilation performance. A key to maximizing the benefit of multi-source data is to strategically select complementary combinations based on sensor characteristics. To this end, an additional experiment was conducted, referred to as the NEW experiment, which assimilates only L- and C-band soil moisture products over densely vegetated regions, and all three bands (L, C, and X) elsewhere. Figure 11 shows the probability density distribution of correlation coefficient differences relative to the CTL for the NEW, L+C, and L+C+X experiments. The distributions for L+C and L+C+X are largely similar, indicating that the inclusion of MWRI (X-band) does not provide a clear advantage over the L+C combination.

In contrast, the NEW experiment exhibits notably better performance. Its mean correlation improvement reaches 0.17, and its probability density in the high-positive range (0.6–0.75) is significantly higher than that of L+C and slightly higher than L+C+X (see right inset of Fig. 11). This indicates that the optimized combination in the NEW experiment improves both the stability and overall effectiveness of the assimilation system. Furthermore, in the negative difference range (–0.2 to –0.1), the NEW experiment shows substantially lower probability density than L+C+X (see left inset), suggesting a reduced risk of performance degradation due to X-band data in densely vegetated areas. These results confirm that the NEW experiment achieves superior assimilation performance by employing a more targeted multi-source data combination strategy.

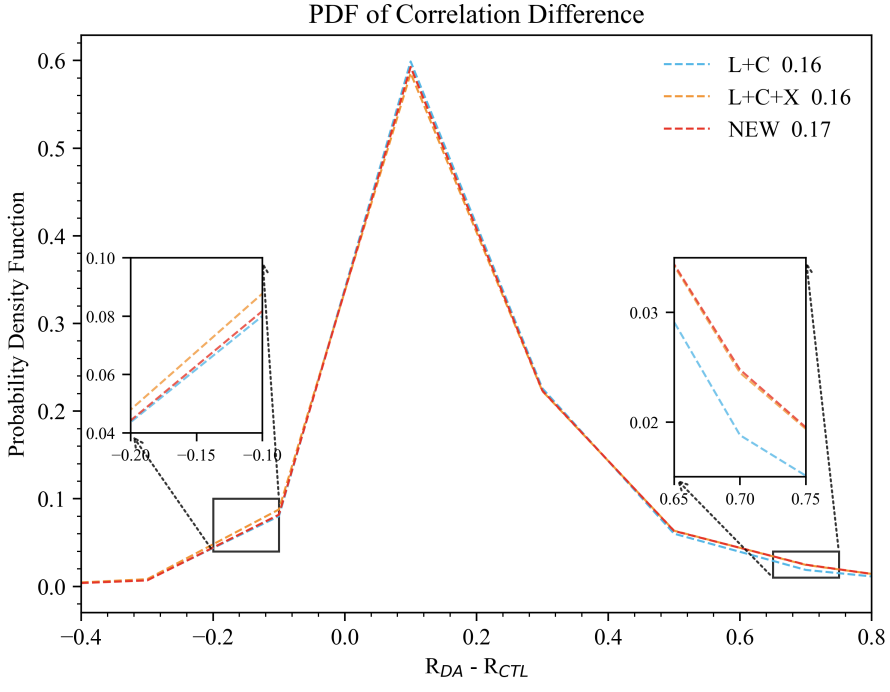

https://doi.org/10.5194/egusphere-2025-5721
Preprint. Discussion started: 23 January 2026

Figure 11: Probability density distributions of the correlation coefficient differences between assimilation experiments (NEW, L+C, and L+C+X) and the CTL, based on in situ observations.

To illuminate spatial heterogeneities in assimilation performance, we leverage existing in-situ networks to focus on two climatologically and ecologically distinct sub-regions of China: the central-west and the southeast. These areas exhibit contrasting vegetation characteristics—the former dominated by low-stature vegetation and bare ground, the latter by dense, high-biomass canopies—thereby providing a natural laboratory for evaluating spatially varying assimilation efficacy. In the CTL, correlation in the central-western region showed a north–south gradient, with a regional average of 0.25, whereas the southeastern region performed better, with an average correlation of 0.52. Data assimilation significantly improved soil moisture simulations in both regions. In the NEW experiment, the correlation in the central-western region increased to 0.5, with especially large improvements (often >0.5) in the north. The southeastern region also improved, with the average correlation rising to 0.58.

https://doi.org/10.5194/egusphere-2025-5721
Preprint. Discussion started: 23 January 2026

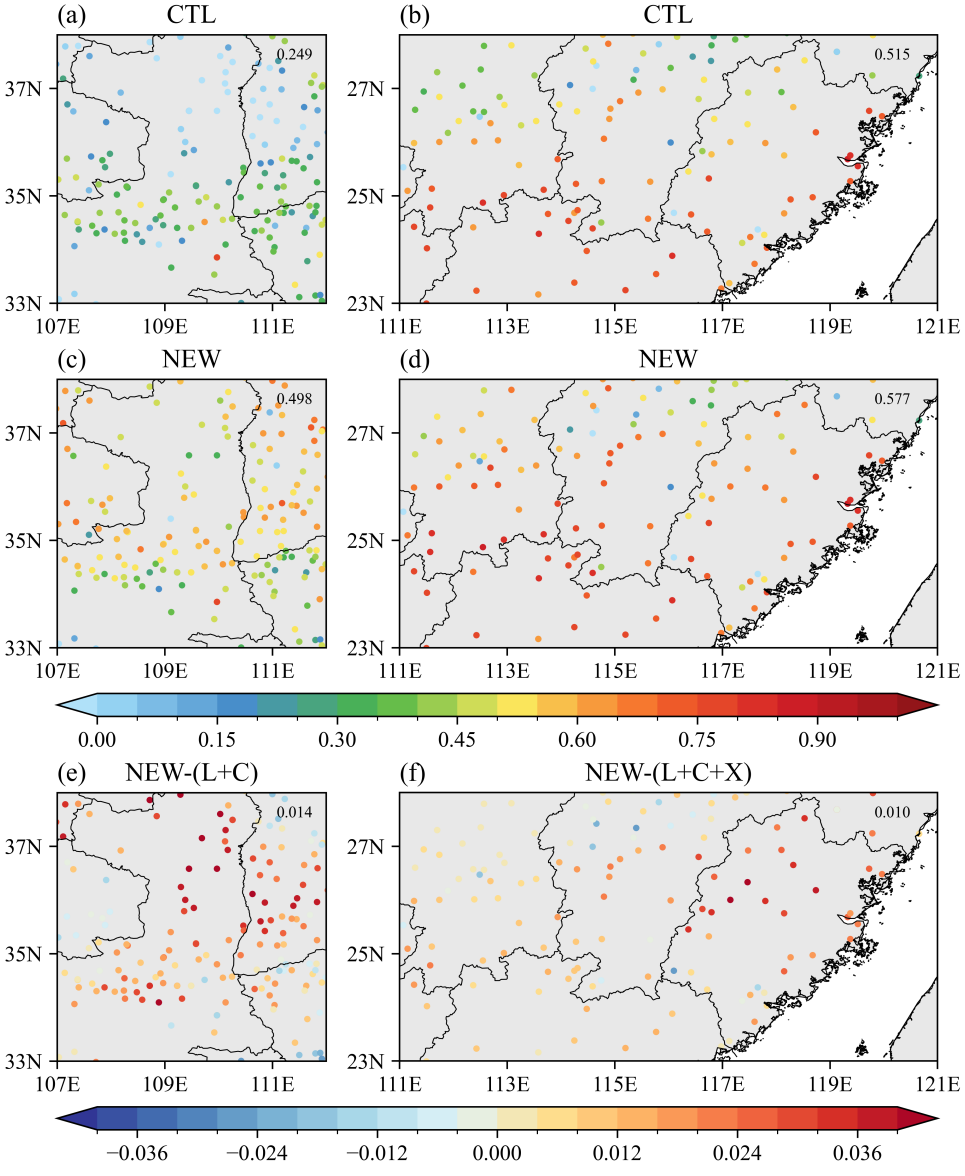

Figure 12: Spatial distribution of correlation coefficients between simulated and observed soil moisture. (a, b) show CTL results for central-west and southeast China, respectively, (c, d) show NEW experiment results for central-west and southeast China, respectively, and (e, f) show correlation differences between the NEW experiment and L+C and between the NEW experiment and L+C+X, respectively.

Unbiased RMSE (ubRMSE) between modeled and observed soil moisture is shown in Figure 13. Compared to the CTL, the NEW experiment exhibited a remarkable reduction in ubRMSE in both regions. In central-western China, the ubRMSE decreased from 0.068 to 0.058, and in southeastern China, it declined from 0.055 to 0.052. ubRMSE differences shows predominantly negative values (blue), indicating that the NEW scheme reduced model error across most areas. However,

https://doi.org/10.5194/egusphere-2025-5721
Preprint. Discussion started: 23 January 2026

localized increases in ubRMSE were also identified, indicating the need for further optimization strategies in multi-satellite data assimilation.

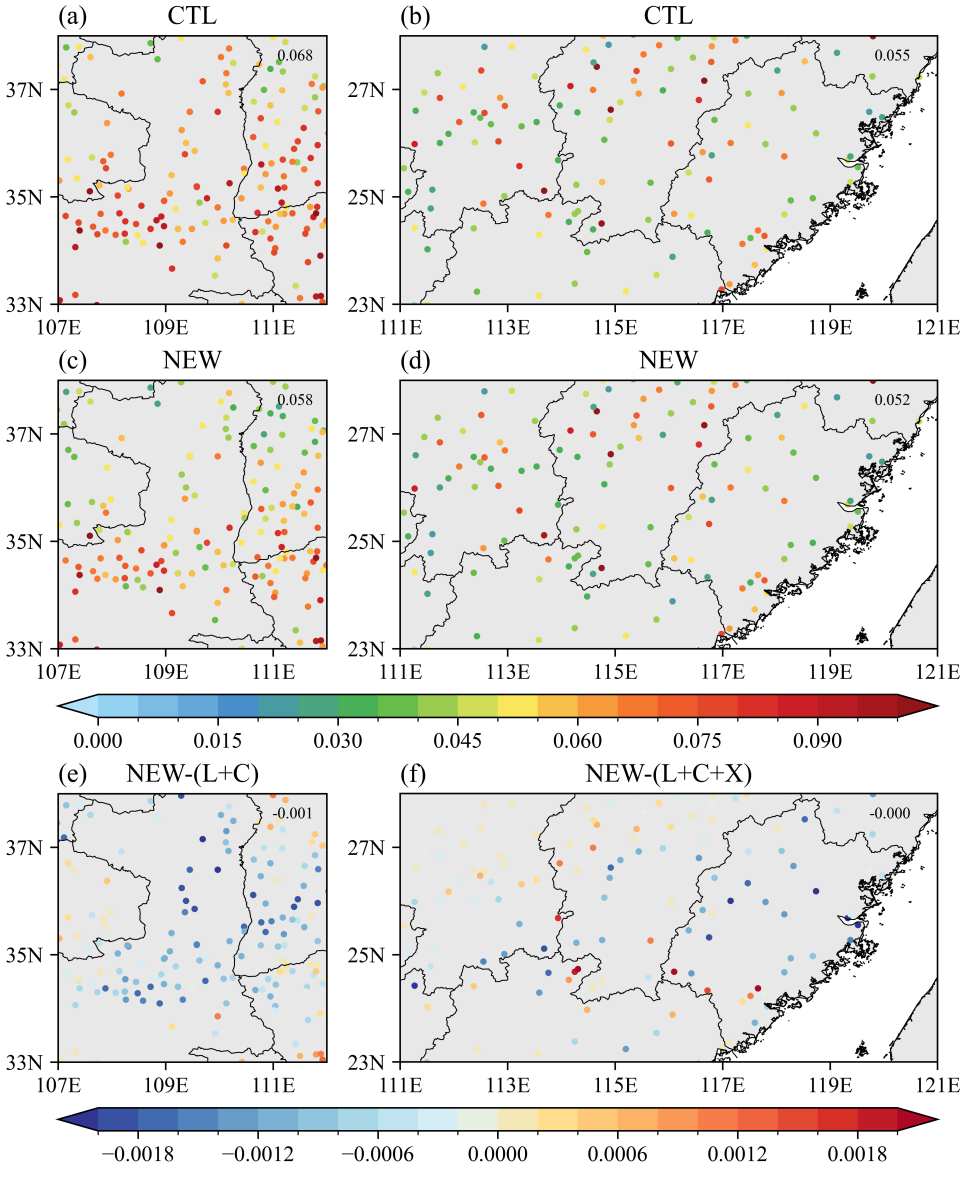

Figure 13: Same as Fig. 12 except for ubRMSE.

https://doi.org/10.5194/egusphere-2025-5721
Preprint. Discussion started: 23 January 2026

5. Summary and Discussion

The effectiveness of assimilating satellite-based soil moisture retrievals in improving LSM performance has been widely recognized. With the rapid advancement of satellite remote sensing technology, numerous microwave radiometer-equipped polar-orbiting meteorological satellites have been launched globally, providing increasingly abundant observational resources. Against this background, effectively leveraging multi-source microwave data has become a key scientific challenge for enhancing land surface simulations. In this study, we develop a vegetation-adaptive framework for constructing optimal multi-satellite assimilation systems. Soil moisture retrievals from sensors operating at different microwave frequencies (SMAP L-band, ASCAT C-band, and MWRI X-band) were assimilated using the SEKF. Beyond systematic evaluation of each frequency band's performance, we established quantitative criteria for optimal sensor combination and developed decision rules for dynamic sensor weighting based on local vegetation characteristics, providing a paradigm shift from volume-driven to complementarity-driven data fusion strategies.

The findings show that assimilating satellite soil moisture products significantly improves simulations of both surface and root-zone soil moisture. However, assimilation performance varies substantially with vegetation type. In densely vegetated regions, assimilating SMAP L-band retrievals consistently yields superior results due to the strong vegetation penetration capability of the L-band. In contrast, in sparsely vegetated high-latitude regions, MWRI (X-band) and ASCAT (C-band) products exhibit higher sensitivity to soil moisture variability and provide better assimilation outcomes. Vegetation-specific evaluation reveals that these differences stem from frequency-dependent vegetation penetration, which affects retrieval accuracy.

Importantly, the results also demonstrate that increasing the number of assimilated satellite products does not always lead to improved performance. The combined assimilation of SMAP and ASCAT outperforms single-sensor assimilation. Further improvement is achieved only when MWRI data are selectively incorporated in regions with low vegetation cover. These results reveal that optimal sensor combination must be vegetation-adaptive. Accordingly, we developed a systematic framework that dynamically selects sensor combinations based on local vegetation conditions, prioritizing SMAP+ASCAT in most regions while conditionally adding MWRI only in sparse vegetation areas. This highlights that the effectiveness of multi-source assimilation depends not only on data volume but also on the complementarity of the assimilated information.

While this study focused primarily on the role of vegetation density, other environmental factors such as terrain elevation, precipitation, and temperature can also influence the retrieval errors of different frequency bands. For instance, terrain-induced variations in local incidence angles can alter the polarization and scattering characteristics of microwave signals, thereby affecting retrieval accuracy (Gibon et al., 2024). Seasonal variations in vegetation cover, rainfall distribution, and temperature may also systematically impact retrieval performance (Liu et al., 2022). Future work should explore the influence of these factors through statistical or machine learning approaches to model their relationships with retrieval errors (Kim et al., 2023). Incorporating such models into multi-sensor assimilation frameworks may further enhance performance.

https://doi.org/10.5194/egusphere-2025-5721
Preprint. Discussion started: 23 January 2026

Finally, this study is based on offline land surface model simulations and does not account for land–atmosphere interactions, which may limit the generalizability of the proposed assimilation strategy in forecasting applications. Future studies should apply and evaluate the assimilation schemes within coupled land–atmosphere systems to better support improvements in weather and climate prediction.

Code and data availability. The Common Land Model (CoLM, version 2014) used in this study was downloaded from the website of the Land–Atmosphere Interaction Research Group at Sun Yat-sen University: http://globalchange.bnu.edu.cn/research/models (Ji et al., 2014, last access: 13 January 2025). SMAP soil moisture data are available from the NASA National Snow and Ice Data Center Distributed Active Archive Center (NSIDC DAAC): https://doi.org/10.5067/BN36FXOMMC4C (O Neill et al., 2023). The ASCAT surface soil moisture data can be downloaded from the EUMETSAT Data Store (https://data.eumetsat.int/data/map/EO:EUM:DAT:METOP:SOMO25, last access: 20 January 2025). The ISMN in-situ soil moisture measurements can be downloaded from the International Soil Moisture Network (https://ismn.earth/en/dataviewer, last access: 11 May 2025). ERA5-Land reanalysis data are available from the Copernicus Climate Data Store (CDS): https://doi.org/10.24381/cds.e2161bac (Muñoz-Sabater, 2019). The code of the Common Land Model (CoLM) version 2014 and the source code of the assimilation system, as well as the data process software codes and the model outputs' data, have been uploaded to Zenodo repositories, which are available at https://doi.org/10.5281/zenodo.17661825 (Bai., 2025).

Author contributions. Xuesong Bai: Writing – review & editing, Writing – original draft, Validation, Formal analysis, Conceptualization. Zhaohui Lin: Writing – review & editing, Supervision, Conceptualization. Zhengkun Qin: Writing – review & editing, Supervision, Conceptualization. Juan Li: Writing – review & editing, Methodology.

Competing interests. The contact author has declared that none of the authors has any competing interests.

Acknowledgements. We acknowledge the High Performance Computing Center of Nanjing University of Information Science & Technology for their support of this work. We acknowledge the use of ChatGPT for assistance with English translation and language polishing during manuscript preparation.

Financial support. This research was supported in part by the National Natural Science Foundation of China under Grants U2442218 and 42375004, and in part by the Hainan Lian Education and Technology Innovation Joint Project under Grant ZDYF2025(LALH)005.

https://doi.org/10.5194/egusphere-2025-5721
Preprint. Discussion started: 23 January 2026

References

Albergel, C., Munier, S., Leroux, D. J., Dewaele, H., Fairbairn, D., Barbu, A. L., Gelati, E., Dorigo, W., Faroux, S., Meurey, C., Le Moigne, P., Decharme, B., Mahfouf, J.-F., and Calvet, J.-C.: Sequential assimilation of satellite-derived vegetation and soil moisture products using SURFEX_v8.0: LDAS-Monde assessment over the Euro-Mediterranean area, Geosci. Model Dev., 10, 3889–3912, https://doi.org/10.5194/gmd-10-3889-2017, 2017.

Bai, X., Qin, Z., Li, J., Zhang, S., and Wang, L.: The Impact of Spatial Dynamic Error on the Assimilation of Soil Moisture Retrieval Products, Remote Sensing, 17, 239, https://doi.org/10.3390/rs17020239, 2025.

Bai, X.: A Preliminary Study on a Synergistic Assimilation Scheme for Multi-band Satellite Soil Moisture Data, Zenodo [data set and code], https://doi.org/10.5281/zenodo.17661825, 2025.

Balsamo, G., Bouyssel, F., and Noilhan, J.: A simplified bi-dimensional variational analysis of soil moisture from screen-level observations in a mesoscale numerical weather-prediction model, Q. J. R. Meteorol. Soc., 130, 895–915, https://doi.org/10.1256/qj.02.215, 2004.

Bartalis, Z., Wagner, W., Naeimi, V., Hasenauer, S., Scipal, K., Bonekamp, H., Figa, J., and Anderson, C.: Initial soil moisture retrievals from the METOP-A Advanced Scatterometer (ASCAT), Geophys. Res. Lett., 34, https://doi.org/10.1029/2007GL031088, 2007.

Brocca, L., Moramarco, T., Melone, F., Wagner, W., Hasenauer, S., and Hahn, S.: Assimilation of surface- and root-zone ASCAT soil moisture products into rainfall-runoff modeling, IEEE Trans. Geosci. Remote Sens., 50, 2542–2555, https://doi.org/10.1109/TGRS.2011.2177468, 2012.

Chambon, P., Mahfouf, J.-F., Audouin, O., Birman, C., Fourrié, N., Loo, C., Martet, M., Moll, P., Payan, C., Pourret, V., and Raspaud, D.: Global Observing System Experiments within the Météo-France 4D-Var Data Assimilation System, Mon. Wea. Rev., 151, 127–143, https://doi.org/10.1175/MWR-D-22-0087.1, 2023.

Chen, F., Crow, W. T., Bindlish, R., Colliander, A., Burgin, M. S., Asanuma, J., and Aida, K.: Global-scale evaluation of SMAP, SMOS and ASCAT soil moisture products using triple collocation, Remote Sens. Environ., 214, 1–13, https://doi.org/10.1016/j.rse.2018.05.008, 2018.

Dai, Y., Zeng, X., Dickinson, R. E., Baker, I., Bonan, G. B., Bosilovich, M. G., Denning, A. S., Dirmeyer, P. A., Houser, P. R., Niu, G., Oleson, K. W., Schlosser, C. A., and Yang, Z.-L.: The Common Land Model, Bulletin of the American Meteorological Society, 84, 1013–1024, https://doi.org/10.1175/BAMS-84-8-1013, 2003.

Das, B., Rathore, P., Roy, D., Chakraborty, D., Bhattacharya, B. K., Mandal, D., Jatav, R., Sethi, D., Mukherjee, J., Sehgal, V. K., Singh, A. K., and Kumar, P.: Ensemble surface soil moisture estimates at farm-scale combining satellite-based optical-thermal-microwave remote sensing observations, Agric. For. Meteorol., 339, 109567, https://doi.org/10.1016/j.agrformet.2023.109567, 2023.

Dash, S. K. and Sinha, R.: A Comprehensive Evaluation of Gridded L-, C-, and X-Band Microwave Soil Moisture Product over the CZO in the Central Ganga Plains, India, Remote Sensing, 14, 1629, https://doi.org/10.3390/rs14071629, 2019.

Dorigo, W., Himmelbauer, I., Aberer, D., Schremmer, L., Petrakovic, I., Zappa, L., Preimesberger, W., Xaver, A., Annor, F., Ardö, J., Baldocchi, D., Bitelli, M., Blöschl, G., Bogena, H., Brocca, L., Calvet, J.-C., Camarero, J. J., Capello, G., Choi, M., Cosh, M. C., van de Giesen, N., Hajdu, I., Ikonen, J., Jensen, K. H., Kanniah, K. D., de Kat, I., Kirchengast, G., Kumar Rai, P., Kyrouac, J., Larson, K., Liu, S., Loew, A., Moghaddam, M., Martínez Fernández, J., Mattar Bader, C., Morbidelli, R., Musial, J. P., Osenga, E., Palecki, M. A., Pellarin, T., Petropoulos, G. P., Pfeil, I., Powers, J., Robock, A., Rüdiger, C., Rummel, U., Strobel, M., Su, Z., Sullivan, R., Tagesson, T., Varlagin, A., Vreugdenhil, M., Walker, J., Wen, J., Wenger, F., Wigneron, J. P., Woods, M., Yang, K., Zeng, Y., Zhang, X., Zreda, M., Dietrich, S., Gruber, A., van Oevelen, P., Wagner, W., Scipal, K., Drusch, M., and Sabia, R.: The International Soil Moisture Network: serving Earth system science for over a decade, Hydrol. Earth Syst. Sci., 25, 5749–5804, https://doi.org/10.5194/hess-25-5749-2021, 2021.

Dorigo, W. A., Scipal, K., Parinussa, R. M., Liu, Y. Y., Wagner, W., de Jeu, R. A. M., and Naeimi, V.: Error characterisation of global active and passive microwave soil moisture datasets, Hydrol. Earth Syst. Sci., 14, 2605–2616, https://doi.org/10.5194/hess-14-2605-2010, 2010.

Draper, C. and Reichle, R.: The impact of near-surface soil moisture assimilation at subseasonal, seasonal, and inter-annual timescales, Hydrol. Earth Syst. Sci., 19, 4831–4844, https://doi.org/10.5194/hess-19-4831-2015, 2015.

Draper, C. S., Mahfouf, J.-F., and Walker, J. P.: An EKF assimilation of AMSR-E soil moisture into the ISBA land surface scheme, J. Geophys. Res., 114, D20104, https://doi.org/10.1029/2008JD011650, 2009.

https://doi.org/10.5194/egusphere-2025-5721
Preprint. Discussion started: 23 January 2026

Drusch, M., Scipal, K., de Rosnay, P., Balsamo, G., Andersson, E., Bougeault, P., and Viterbo, P.: Towards a Kalman Filter based soil moisture analysis system for the operational ECMWF Integrated Forecast System, Geophys. Res. Lett., 36, L10401, https://doi.org/10.1029/2009GL037716, 2009.

El Hajj, M., Baghdadi, N., Zribi, M., and Bazzi, H.: Synergic Use of Sentinel-1 and Sentinel-2 Images for Operational Soil Moisture Mapping at High Spatial Resolution over Agricultural Areas, Remote Sensing, 9, 1292, https://doi.org/10.3390/rs9121292, 2017.

Entekhabi, D., Njoku, E. G., O'Neill, P. E., Kellogg, K. H., Crow, W. T., Edelstein, W. N., Entin, J. K., Goodman, S. D., Jackson, T. J., Johnson, J., Kimball, J., Piepmeier, J. R., Koster, R. D., Martin, N., McDonald, K. C., Moghaddam, M., Moran, S., Reichle, R., Shi, J. C., Spencer, M. W., Thurman, S. W., Tsang, L., and Van Zyl, J.: The Soil Moisture Active Passive (SMAP) Mission, Proc. IEEE, 98, 704–716, https://doi.org/10.1109/JPROC.2010.2043918, 2010.

Gibon, F., Mialon, A., Richaume, P., Rodríguez-Fernández, N., Aberer, D., Boresch, A., Crapolicchio, R., Dorigo, W., Gruber, A., Himmelbauer, I., Preimesberger, W., Sabia, R., Stradiotti, P., Tercjak, M., and Kerr, Y. H.: Estimating the uncertainties of satellite derived soil moisture at global scale, Science of Remote Sensing, 10, 100147, https://doi.org/10.1016/j.srs.2024.100147, 2024.

Herbert, C., de Rosnay, P., Weston, P., and Fairbairn, D.: Towards unified land data assimilation at ECMWF: Soil and snow temperature analysis in the SEKF, Quart J Royal Meteoro Soc, 150, 4133–4155, https://doi.org/10.1002/qj.4808, 2024.

Hess, R.: Assimilation of screen-level observations by variational soil moisture analysis, Meteorol. Atmos. Phys., 77, 145–154, https://doi.org/10.1007/s007030170023, 2001.

Jackson, T. J. and Schmugge, T. J.: Vegetation effects on the microwave emission of soils, Remote Sens. Environ., 36, 203–212, https://doi.org/10.1016/0034-4257(91)90057-D, 1991.

Ji, D., Wang, L., Feng, J., Wu, Q., Cheng, H., Zhang, Q., Yang, J., Dong, W., Dai, Y., Gong, D., Zhang, R.-H., Wang, X., Liu, J., Moore, J. C., Chen, D., and Zhou, M.: Description and basic evaluation of Beijing Normal University Earth System Model (BNU-ESM) version 1, Geosci. Model Dev., 7, 2039–2064, https://doi.org/10.5194/gmd-7-2039-2014, 2014.

Kang, C. S., Zhao, T., Shi, J., Cosh, M. H., Chen, Y., Starks, P. J., Collins, C. H., Wu, S., Sun, R., and Zheng, J.: Global Soil Moisture Retrievals From the Chinese FY-3D Microwave Radiation Imager, IEEE Trans. Geosci. Remote Sens., 59, 4018–4032, https://doi.org/10.1109/TGRS.2020.3019408, 2021.

Kerr, Y. H., Waldteufel, P., Wigneron, J.-P., Delwart, S., Cabot, F., Boutin, J., Escorihuela, M.-J., Font, J., Reul, N., Gruhier, C., Juglea, S. E., Drinkwater, M. R., Hahne, A., Martín-Neira, M., and Mecklenburg, S.: The SMOS Mission: New Tool for Monitoring Key Elements ofthe Global Water Cycle, Proc. IEEE, 98, 666–687, https://doi.org/10.1109/JPROC.2010.2043032, 2010.

Kerr, Y. H., Waldteufel, P., Richaume, P., Wigneron, J. P., Ferrazzoli, P., Mahmoodi, A., Al Bitar, A., Cabot, F., Gruhier, C., Juglea, S. E., Leroux, D., Mialon, A., and Delwart, S.: The SMOS Soil Moisture Retrieval Algorithm, IEEE Trans. Geosci. Remote Sens., 50, 1384–1403, https://doi.org/10.1109/TGRS.2012.2184548, 2012.

Khaki, M., Hoteit, I., Kuhn, M., Forootan, E., and Awange, J.: Assessing data assimilation frameworks for using multi-mission satellite products in a hydrological context, Science of The Total Environment, 647, 1031–1043, https://doi.org/10.1016/j.scitotenv.2018.08.032, 2019.

Kim, H., Parinussa, R., Konings, A. G., Wagner, W., Cosh, M. H., Lakshmi, V., Zohaib, M., and Choi, M.: Global-scale assessment and combination of SMAP with ASCAT (active) and AMSR2 (passive) soil moisture products, Remote Sens. Environ., 204, 260–275, https://doi.org/10.1016/j.rse.2017.10.026, 2018.

Kim, H., Crow, W., Li, X., Wagner, W., Hahn, S., and Lakshmi, V.: True global error maps for SMAP, SMOS, and ASCAT soil moisture data based on machine learning and triple collocation analysis, Remote Sens. Environ., 298, 113776, https://doi.org/10.1016/j.rse.2023.113776, 2023.

Kolassa, J., Reichle, R. H., and Draper, C. S.: Merging active and passive microwave observations in soil moisture data assimilation, Remote Sens. Environ., 191, 117–130, https://doi.org/10.1016/j.rse.2017.01.015, 2017.

Koster, R. D., Schubert, S. D., DeAngelis, A. M., Molod, A. M., and Mahanama, S. P.: Using a Simple Water Balance Framework to Quantify the Impact of Soil Moisture Initialization on Subseasonal Evapotranspiration and Air Temperature Forecasts, J. Hydrometeorol., 21, 1705–1722, https://doi.org/10.1175/JHM-D-20-0007.1, 2020.

Kumar, S. V., PETERSLIDARD, C., TIAN, Y., HOUSER, P., GEIGER, J., OLDEN, S., LIGHTY, L., EASTMAN, J., DOTY, B., and DIRMEYER, P.: Land information system: An interoperable framework for high resolution land surface modeling, Environ. Modell. Softw., 21, 1402–1415, https://doi.org/10.1016/j.envsoft.2005.07.004, 2006.

https://doi.org/10.5194/egusphere-2025-5721
Preprint. Discussion started: 23 January 2026

Kumar, S. V., Reichle, R. H., Koster, R. D., Crow, W. T., and Peters-Lidard, C. D.: Role of Subsurface Physics in the Assimilation of Surface Soil Moisture Observations, J. Hydrometeorol., 10, 1534–1547, https://doi.org/10.1175/2009JHM1134.1, 2009.

Kumar, S. V., Peters-Lidard, C. D., Mocko, D., Reichle, R., Liu, Y., Arsenault, K. R., Xia, Y., Ek, M., Riggs, G., Livneh, B., and Cosh, M.: Assimilation of Remotely Sensed Soil Moisture and Snow Depth Retrievals for Drought Estimation, J. Hydrometeorol., 15, 2446–2469, https://doi.org/10.1175/JHM-D-13-0132.1, 2014.

Lawrence, D. M., Fisher, R. A., Koven, C. D., Oleson, K. W., Swenson, S. C., Bonan, G., Collier, N., Ghimire, B., van Kampenhout, L., Kennedy, D., Kluzek, E., Lawrence, P. J., Li, F., Li, H., Lombardozzi, D., Riley, W. J., Sacks, W. J., Shi, M., Vertenstein, M., Wieder, W. R., Xu, C., Ali, A. A., Badger, A. M., Bisht, G., van den Broeke, M., Brunke, M. A., Burns, S. P., Buzan, J., Clark, M., Craig, A., Dahlin, K., Drewniak, B., Fisher, J. B., Flanner, M., Fox, A. M., Gentine, P., Hoffman, F., Keppel-Aleks, G., Knox, R., Kumar, S., Lenaerts, J., Leung, L. R., Lipscomb, W. H., Lu, Y., Pandey, A., Pelletier, J. D., Perket, J., Randerson, J. T., Ricciuto, D. M., Sanderson, B. M., Slater, A., Subin, Z. M., Tang, J., Thomas, R. Q., Val Martin, M., and Zeng, X.: The Community Land Model Version 5: Description of New Features, Benchmarking, and Impact of Forcing Uncertainty, J. Adv. Model. Earth Syst., 11, 4245–4287, https://doi.org/10.1029/2018MS001583, 2019.

Li, J., Qin, Z., Liu, G., and Huang, J.: Added Benefit of the Early-Morning-Orbit Satellite Fengyun-3E on the Global Microwave Sounding of the Three-Orbit Constellation, Adv. Atmos. Sci., 41, 39–52, https://doi.org/10.1007/s00376-023-2388-z, 2024.

Li, X., Chen, G., Liu, X., Liang, X., Wang, S., Chen, Y., Pei, F., and Xu, X.: A New Global Land-Use and Land-Cover Change Product at a 1-km Resolution for 2010 to 2100 Based on Human–Environment Interactions, Annals of the American Association of Geographers, 107, 1040–1059, https://doi.org/10.1080/24694452.2017.1303357, 2017.

Lin, L., Ebtehaj, A. M., Wang, J., and Bras, R. L.: Soil moisture background error covariance and data assimilation in a coupled land-atmosphere model, Water Resour. Res., 53, 1309–1335, https://doi.org/10.1002/2015WR017548, 2017.

Lin, Z., Liu, H., Xie, Z., Wang, A., and Liu, S.: The Curvelet Transform, Chinese Journal of Atmospheric Sciences, 27, 118–133, https://doi.org/10.3878/j.issn.1006-9895.2008.04.19, 2010.

Liu, D. and Mishra, A. K.: Performance of AMSR_E soil moisture data assimilation in CLM4.5 model for monitoring hydrologic fluxes at global scale, J. Hydrol., 547, 67–79, https://doi.org/10.1016/j.jhydrol.2017.01.036, 2017.

Liu, W., Wang, J., Xu, F., Li, C., and Xian, T.: Validation of Four Satellite-Derived Soil Moisture Products Using Ground-Based In Situ Observations over Northern China, Remote Sensing, 14, 1419, https://doi.org/10.3390/rs14061419, 2022.

Liu, Y., Peters-Lidard, C. D., Kumar, S., Foster, J. L., Shaw, M., Tian, Y., and Fall, G. M.: Assimilating satellite-based snow depth and snow cover products for improving snow predictions in Alaska, Adv. Water Res., 54, 208–227, https://doi.org/10.1016/j.advwatres.2013.02.005, 2013.

Mousa, B. G. and Shu, H.: Spatial Evaluation and Assimilation of SMAP, SMOS, and ASCAT Satellite Soil Moisture Products Over Africa Using Statistical Techniques, Earth Space Sci., 7, e2019EA000841, https://doi.org/10.1029/2019EA000841, 2020.

Muñoz-Sabater, J.: ERA5-Land hourly data from 1950 to present, Copernicus Climate Change Service (C3S) Climate Data Store (CDS) [data set], https://doi.org/10.24381/cds.e2161bac, 2019.

Njoku, E., Stacey, J., and Barath, F.: The Seasat scanning multichannel microwave radiometer (SMMR): Instrument description and performance, IEEE J. Ocean. Eng., 5, 100–115, https://doi.org/10.1109/JOE.1980.1145458, 1980.

Njoku, E. G. and Entekhabi, D.: Passive microwave remote sensing of soil moisture, J. Hydrol., 184, 101–129, https://doi.org/10.1016/0022-1694(95)02970-2, 1996.

Njoku, E. G., Jackson, T. J., Lakshmi, V., Chan, T. K., and Nghiem, S. V.: Soil moisture retrieval from AMSR-E, IEEE Trans. Geosci. Remote Sens., 41, 215–229, https://doi.org/10.1109/TGRS.2002.808243, 2003.

ONeill, P., Chan, S., Njoku, E., Jackson, T., Bindlish, R., Chaubell, J., and Colliander, A.: SMAP enhanced L2 radiometer half-orbit 9 km EASE-grid soil moisture, version 6, NASA National Snow and Ice Data Center Distributed Active Archive Center [data set], https://doi.org/10.5067/BN36FXOMMC4C, 2023.

Owe, M., de Jeu, R., and Walker, J.: A methodology for surface soil moisture and vegetation optical depth retrieval using the microwave polarization difference index, IEEE Trans. Geosci. Remote Sens., 39, 1643–1654, https://doi.org/10.1109/36.942542, 2001.

https://doi.org/10.5194/egusphere-2025-5721
Preprint. Discussion started: 23 January 2026

Paloscia, S., Pettinato, S., Santi, E., Notarnicola, C., Pasolli, L., and Reppucci, A.: Soil moisture mapping using Sentinel-1 images: Algorithm and preliminary validation, Remote Sens. Environ., 134, 234–248, https://doi.org/10.1016/j.rse.2013.02.027, 2013.

Parinussa, R. M., Holmes, T. R. H., Wanders, N., Dorigo, W. A., and de Jeu, R. A. M.: A Preliminary Study toward Consistent Soil Moisture from AMSR2, J. Hydrometeorol., 16, 932–947, https://doi.org/10.1175/JHM-D-13-0200.1, 2015.

Peng, J., Albergel, C., Balenzano, A., Brocca, L., Cartus, O., Cosh, M. H., Crow, W. T., Dabrowska-Zielinska, K., Dadson, S., Davidson, M. W. J., de Rosnay, P., Dorigo, W., Gruber, A., Hagemann, S., Hirschi, M., Kerr, Y. H., Lovergine, F., Mahecha, M. D., Marzahn, P., Mattia, F., Musial, J. P., Preuschmann, S., Reichle, R. H., Satalino, G., Silgram, M., van Bodegom, P. M., Verhoest, N. E. C., Wagner, W., Walker, J. P., Wegmüller, U., and Loew, A.: A roadmap for high-resolution satellite soil moisture applications – confronting product characteristics with user requirements, Remote Sens. Environ., 252, 112162, https://doi.org/10.1016/j.rse.2020.112162, 2021.

Piepmeier, J. R., Focardi, P., Horgan, K. A., Knuble, J., Ehsan, N., Lucey, J., Brambora, C., Brown, P. R., Hoffman, P. J., French, R. T., Mikhaylov, R. L., Kwack, E.-Y., Slimko, E. M., Dawson, D. E., Hudson, D., Peng, J., Mohammed, P. N., De Amici, G., Freedman, A. P., Medeiros, J., Sacks, F., Estep, R., Spencer, M. W., Chen, C. W., Wheeler, K. B., Edelstein, W. N., O'Neill, P. E., and Njoku, E. G.: SMAP L-Band Microwave Radiometer: Instrument Design and First Year on Orbit, IEEE Trans. Geosci. Remote Sens., 55, 1954–1966, https://doi.org/10.1109/TGRS.2016.2631978, 2017.

Santanello, J. A., Kumar, S. V., Peters-Lidard, C. D., and Lawston, P. M.: Impact of Soil Moisture Assimilation on Land Surface Model Spinup and Coupled Land–Atmosphere Prediction, J. Hydrometeorol., 17, 517–540, https://doi.org/10.1175/JHM-D-15-0072.1, 2016.

Seneviratne, S. I., Corti, T., Davin, E. L., Hirschi, M., Jaeger, E. B., Lehner, I., Orlowsky, B., and Teuling, A. J.: Investigating soil moisture–climate interactions in a changing climate: A review, Earth Sci. Rev., 99, 125–161, https://doi.org/10.1016/j.earscirev.2010.02.004, 2010.

Seo, E., Lee, M.-I., and Reichle, R. H.: Assimilation of SMAP and ASCAT soil moisture retrievals into the JULES land surface model using the Local Ensemble Transform Kalman Filter, Remote Sens. Environ., 253, 112222, https://doi.org/10.1016/j.rse.2020.112222, 2021.

Shan, X., Steele-Dunne, S., Hahn, S., Wagner, W., Bonan, B., Albergel, C., Calvet, J.-C., and Ku, O.: Assimilating ASCAT normalized backscatter and slope into the land surface model ISBA-A-gs using a Deep Neural Network as the observation operator: Case studies at ISMN stations in western Europe, Remote Sens. Environ., 308, 114167, https://doi.org/10.1016/j.rse.2024.114167, 2024.

Shen, W., Lin, Z., Qin, Z., and Li, J.: Development and preliminary validation of a land surface image assimilation system based on the Common Land Model, Geosci. Model Dev., 17, 3447–3465, https://doi.org/10.5194/gmd-17-3447-2024, 2024.

Sun, Y., Huang, S., Ma, J., Li, J., Li, X., Wang, H., Chen, S., and Zang, W.: Preliminary Evaluation of the SMAP Radiometer Soil Moisture Product over China Using In Situ Data, Remote Sensing, 9, 292, https://doi.org/10.3390/rs9030292, 2017.

Taylor, C. M.: Detecting soil moisture impacts on convective initiation in Europe, Geophys. Res. Lett., 42, 4631–4638, https://doi.org/10.1002/2015GL064030, 2015.

Tian, J., Lu, H., Yang, K., Qin, J., Zhao, L., Zhou, J., Jiang, Y., and Ma, X.: Quick estimation of parameters for the land surface data assimilation system and its influence based on the extended Kalman filter and automatic differentiation, Sci. China Earth Sci., 66, 2546–2562, https://doi.org/10.1007/s11430-022-1180-8, 2023.

Wanders, N., Karssenberg, D., de Roo, A., de Jong, S. M., Bierkens, M. F. P., Han, C., Brdar, S., and Kollet, S.: Response of Convective Boundary Layer and Shallow Cumulus to Soil Moisture Heterogeneity: A Large-Eddy Simulation Study, J. Adv. Model. Earth Syst., 11, 4305–4322, https://doi.org/10.1029/2019MS001772, 2019a.

Wanders, N., Karssenberg, D., de Roo, A., de Jong, S. M., and Bierkens, M. F. P.: The suitability of remotely sensed soil moisture for improving operational flood forecasting, Hydrol. Earth Syst. Sci., 18, 2343–2357, https://doi.org/10.5194/hess-18-2343-2014, 2019b.

Wigneron, J.-P., Jackson, T. J., O'Neill, P., De Lannoy, G., de Rosnay, P., Walker, J. P., Ferrazzoli, P., Mironov, V., Bircher, S., Grant, J. P., Kurum, M., Schwank, M., Munoz-Sabater, J., Das, N., Royer, A., Al-Yaari, A., Al Bitar, A., Fernandez-Moran, R., Lawrence, H., Mialon, A., Parrens, M., Richaume, P., Delwart, S., and Kerr, Y.: Modelling the passive microwave signature from land surfaces: A review of recent results and application to the L-band SMOS & SMAP soil moisture retrieval algorithms, Remote Sens. Environ., 192, 238–262, https://doi.org/10.1016/j.rse.2017.01.024, 2017.

https://doi.org/10.5194/egusphere-2025-5721
Preprint. Discussion started: 23 January 2026

Zapotocny, T. H., Jung, J. A., Le Marshall, J. F., and Treadon, R. E.: A Two-Season Impact Study of Satellite and In Situ Data in the NCEP Global Data Assimilation System, Wea. Forecasting, 22, 887–909, https://doi.org/10.1175/WAF1025.1, 2007.

Zhan, Y. and Lin, Z.: The relationship between June precipitation over mid-lower reaches of the Yangtze River basin and spring soil moisture over the East Asian monsoon region, Acta Meteorol. Sin., 25, 355–363, https://doi.org/10.1007/s13351-011-0310-6, 2011.

Zhan, Y., Z. Lin, F. Tian, M. Cao, and Y. Xu: The Spatio-Temporal Characteristics of Soil Moisture and Its Memory over Huaihe River Basin, Advances in Meteorological Science and Technology, 10, 87–96, https://doi.org/10.3969/j.issn.2095-1973.2020.05.014, 2020 (in Chinese).

Zhang, Y., Liang, S., Ma, H., He, T., Wang, Q., Li, B., Xu, J., Zhang, G., Liu, X., and Xiong, C.: Generation of global 1 km daily soil moisture product from 2000 to 2020 using ensemble learning, Earth Syst. Sci. Data, 15, 2055–2079, https://doi.org/10.5194/essd-15-2055-2023, 2002.

Zhao, T., Shi, J., Entekhabi, D., Jackson, T. J., Hu, L., Peng, Z., Yao, P., Li, S., and Kang, C. S.: Retrievals of soil moisture and vegetation optical depth using a multi-channel collaborative algorithm, Remote Sens. Environ., 257, 112321, https://doi.org/10.1016/J.RSE.2021.112321, 2021.

Zhou, J., Zuo, Z., Rong, X., Li, K., Zhang, J., Yang, K., and Wu, L.: The Role of Soil Moisture Feedbacks in Future Summer Temperature Change over East Asia, JGR Atmospheres, 124, 12034–12056, https://doi.org/10.1029/2018JD029670, 2019.

Zhou, J., Zuo, Z., and Rong, X.: Comparison of the effects of soil moisture and El Niño on summer precipitation in eastern China, Sci. China Earth Sci., 63, 267–278, https://doi.org/10.1007/s11430-018-9469-6, 2020.

Zhu, Y., Li, X., Pearson, S., Wu, D., Sun, R., Johnson, S., Wheeler, J., and Fang, S.: Evaluation of Fengyun-3C Soil Moisture Products Using In-Situ Data from the Chinese Automatic Soil Moisture Observation Stations: A Case Study in Henan Province, China, Water, 11, 248, https://doi.org/10.3390/w11020248, 2019.

Zribi, M.: Surface soil moisture estimation from the synergistic use of the (multi-incidence and multi-resolution) active microwave ERS Wind Scatterometer and SAR data, Remote Sens. Environ., 86, 30–41, https://doi.org/10.1016/S0034-4257(03)00065-8, 2003.